Fly Me to the Moon - For All Mankind

Julius A. Birch

Unaffiliated

(Dated: October 18, 2015)

Apollo flights represent one of the most remarkable achievements of science and technology in the last millennium. Yet, to this day, there are people who are unconvinced that we as a species have set foot on the Moon. This disbelief finds a way to popular culture through movies like "Interstellar" (2014), in which a character claims that "... the flights to the Moon were faked to bankrupt the Soviets," or the upcoming movie "The Martian," in which the main character ridicules Apollo 11 exclaiming "... take that Neil Armstrong!"

In this report we consider some of the most criticized features of the Apollo 11 and 17 Missions that have surfaced in public in the last 45 or so years. We interpret these features in terms of the opposite underlying physical models. One applies if the action were taking place on the way to the Moon, and the other if everything were staged on Earth and perhaps scaled down. What follows may help us decide whether we indeed flew to the Moon - for all mankind. Or not.

Contents

1. WHO'S THAT FLYIN' UP THERE?

Liftoff of the Apollo 17 Lunar Module on December 9, 1972, from Taurus-Littrow Valley on the Moon was recorded by a video camera on the Lunar Roving Vehicle (LRV). The LRV was parked some 120m eastward on the side of a hill, as shown in Fig. 1 from Ref. [1]. The LRV was positioned at higher ground than the Lunar Module, with the Sun approximately behind the camera. We remark that in the NASA reference images of the landing site [2] the Sun is in the west. Interestingly, the camera, which could zoom-out and tilt, was remotely controlled by the Earth ground control [3].

Since the 1970's, speculations have been circulating in the public as to whether the video recording shows liftoff of the Apollo 17 Lunar Module from the Moon, or a staged event occurring elsewhere.something else somewhere else. Some of these speculations can be put to rest through analysis of the video recording of the liftoff.

The purpose of this section is to extract the first 2 seconds of the liftoff dynamics of the Apollo 17 Lunar Module Ascent Stage (LMAS) from the video recording, and to compare it to the values published by NASA in different media. Starting from the equation of motion of a rocket lifting off a planetary surface, we introduce assumptions that allow us to write its short-time solution as a special third- and forth-degree polynomial in time which we call the Jerk (J) and the Snap/Jerk (S/J) model, respectively. The short-time solution then influences the parameters of the constant acceleration motion, which is the long-time solution. We then analyze 21 frames extracted from the video recording at the rate of 10 frames-per-second (fps), to find the height the LMAS gains as a function of time, the so-called, "liftoff" curve. Finally, by fitting the models to the liftoff curve, we find the propulsion parameters and discuss the dynamics of liftoff the video recording depicts.

1.1. Liftoff in Theory

The one-dimensional rocket equation is a standard fare in any text-book on analytical mechanics [4]. Here, we are interested in a rocket lifting off a planet that provides constant gravity g. Let the rocket mass be $m = m(t)$, and let the propellent be expelled from the rocket engine combustion chamber at mass rate $\dot{m}_p(t)$ with the velocity w relative to the rocket. We assume that the planet has no atmosphere, so the motion is described in terms of the rocket vertical velocity $v = v(t)$

as, [5]

$$\dot{v} = \frac{\dot{m}_p\, w}{m(t)} + \frac{p_e\, A_e}{m(t)} - g. \tag{1.1}$$

We remark while the rocket is sitting on the ground the right-hand-side of Eq. (1.1) cannot be smaller than zero, meaning that the rocket remains stationary on the surface. Here, p_e is the pressure of the propellent at the exit of the nozzle, while A_e is the surface of the nozzle at the exit. We simplify Eq. (1.1) as,

$$\dot{v} = \frac{F_{th}(t)}{m(t)} - g, \tag{1.2}$$

where $F_{th} = F_{th}(t)$ is the engine thrust in vacuum, which we allow to vary in time.

For the purpose of our analysis, we split the liftoff dynamics to the initial short-time period, and the subsequent long-time period. We refer to the initial short-time period as the "warm-up". Let us assume that the vessel is initially at rest, and that its rocket engine starts propulsion at time $t = 0$. This is not necessarily the time at which the liftoff starts as it may take time for the rocket engine to produce enough thrust to counter-act gravity. We introduce the warm-up time $t_1 \geq 0$, at which the rocket engine reaches its full (maximal) thrust. The time instant t_1 thus separates the short-time from the long-time period.

First we approximate the warm-up through $F_{th}(t)$ linearly increasing for the duration of warm-up time t_1 and as constant P thereafter,

$$F_{th}(t) = \begin{cases} 0, & \text{for} \quad t \leq 0 \\ \frac{P}{t_1} \cdot t, & \text{for} \quad 0 \leq t \leq t_1, \\ P & \text{for} \quad t_1 \leq t. \end{cases} \tag{1.3}$$

The liftoff starts when the rocket begins to move at time t_0, such that $F_{th}(t) \geq m(t)\, g$, for $t \geq t_0$. From our linear model of thrust we find $t_0 \approx m\, g\, t_1 / P$. For comparison, [6] the Ascent Propulsion System (APS) featured in the Lunar Modules of the Apollo missions had only "on" and "off" states, where the transition between the two states occured in near step-like fashion with the delay time of 0.3 s. In terms of our linear model (1.3) this is written as $t_0 \approx t_1 \approx 0$, with P/t_1 some large number, where the start command to the engine was issued at $t' \approx -0.3$ s.

From the properties of the APS [7, 8], some of which we summarize in Tbl. I, we can neglect the change in the total mass of the LMAS for the 2 seconds of liftoff we are interested in, and so

approximate the LMAS mass with its initial mass $m(t) \approx m_0^{AS}$. This allows us to find the vertical acceleration of the LMAS $\dot{v}_A$ as,

$$\dot{v}_a(t) = \begin{cases} 0, & \text{for} \quad t \leq t_0 \\ j_A \cdot (t - t_0), & \text{for} \quad t_0 \leq t \leq t_1, \\ j_A \cdot (t_1 - t_0), & \text{for} \quad t_1 \leq t. \end{cases} , \tag{1.4}$$

where we have introduced *jerk*, $j = d^3x/dt^3$. We refer to Eq. (1.4) as the J-Model of warm-up. After the warm-up time, $t \geq t_1$, the ascent continues with approximately constant acceleration,

$$a_{max} = j_A \cdot t_1 = \left(\frac{F_{th}}{m_0^{AS} g} - 1 \right) \cdot g \approx 1.95 \text{ m} \cdot \text{s}^{-2}. \tag{1.5}$$

Because of $t_0 \approx t_1 \approx 0$, in Apollo 17 liftoff a_{max} is achieved immediately. As at time $t = 0$ the LMAS is at rest, its vertical position is thus described by

$$X(t) = \frac{a_{max}}{2} t^2. \tag{1.6}$$

In their numerical simulation of Apollo 17 lunar orbit insertion Braeunig [9] reports $X(2 \text{ s}) = 3.0$ m, whereas Eq. (1.6) reads $X(2 \text{ s}) \approx 3.9$ m. This implies that in Braeunig's simulation the Ascent Propulsion System transitions from zero to full thrust with a delay of 0.25 s, in full accord with [6].

Next we anticipate that the J-Model of the rocket engine thrust might not be sufficient, because it constrains the warm-up transients to $j \geq 0$. One way to better capture the transients is to introduce an additional parameter *snap*, $s = \frac{dj}{dt}(t) = \frac{d^2\ddot{x}}{dt^2}(t)$, so that the acceleration during warm-up is:

$$\dot{v}_a(t) = \begin{cases} 0, & \text{for} \quad t \leq t_0 \\ \frac{s}{2}(t - t_0)^2 + j \cdot (t - t_0), & \text{for} \quad t_0 \leq t \leq t_1, \\ \frac{s}{2}(t_1 - t_0)^2 + j \cdot (t_1 - t_0), & \text{for} \quad t_1 \leq t, \end{cases} \tag{1.7}$$

which we refer to as the S/J-Model of warm-up.

Finally, the long term behavior that ensues following the warm-up is best described by the constant acceleration motion,

$$x(t) = \frac{1}{2} \ddot{x}(t_1) (t - t_1)^2 + \dot{x}(t_1) \cdot (t - t_1) + x(t_1), \text{ for } t > t_1, \tag{1.8}$$

where its parameters, namely $\ddot{x}(t_1)$, $\dot{x}(t_1)$ and $x(t_1)$, are fully determined by the warm-up.

When fitting the liftoff curve to the models we see that the J-Model (1.4) has three parameters (j, t_0, t_1), the S/J-Model (1.7) has four (s, j, t_0, t_1), as does the constant acceleration model $(t_1, \ddot{x}_1(t_1), \dot{x}_1(t_1)$ and $x_1(t_1))$. In other words, even though the S/J model appears to be more complicated than the constant acceleration motion, they both have the same number of parameters.

1.2. Liftoff Curve

Processing of Images: The web site YouTube provides the video recording of Apollo 17 liftoff [10] in Adobe-Flash format. We use another web service [11] to download it for us, and to convert it to AVI format. The converted file is then downloaded to our workstation under the name `Apollo_17_Lunar_Liftoff_high.avi`. We analyze the file using the software package FFmpeg [12], and find it comprised of color images 480x360 (width-by-height) pixels recorded at rate $r = 25$ fps. We then convert the video recording to a set of images at the rate $r = 10$ fps [50]. As a result of conversion, we get the images numbered 1,2,3..., where the increments of 1 indicate the time stamp of an image to be $\Delta t = 1/r$ greater then the previous one, with image 00001 being the first. Accordingly, one can determine the absolute time stamp of the image in the video recording as $(n-1)/r$, where n is the index image. We find that at the rate $r = 10$ fps, the first two seconds of liftoff are depicted in 21 images numbered $[363 : 383]_{10}$[51], where the subscript next to the image number or range indicates the extraction rate. For the reader's convinience, in Fig. 2 we provide the reference image 363_{10}, while in Fig. 3 we combine the images $[364 : 383]_{10}$.

We choose as $t = 0$ the image 363_{10} as in the subsequent images the motion of the LMAS is obvious and the Moon surface disappears in the dust cloud. Simultaneously, the images 364_{10} onward begin to show the effects of a continuous zoom-out. [13]

We limit our analysis to the first 2 seconds, as after that point the camera begins to tilt.

Extraction of liftoff curve: In each of the images $[363 : 383]_{10}$ we locate 5 points:

H_1 horizon point No. 1, on the left from LM where the ridge lines of the left hill (presumably, Horatio) and of the right hill (presumably, Camelot) meet;

H_2 horizon point No. 2, on the right from LM at the top of the right hill (Camelot);

L_1 leg point No. 1, bright section at the top of the left leg of the LMDS when facing it on the picture;

M_1 LMAS point No. 1, top left corner of the bright surface of the AS;

M_3 LMAS point No. 3, bottom left corner of the bright surface of the AS.

In Fig. 2 we show these five points on the reference image 363_{10}. In Tbl. II we give the Y-pixel coordinates of each of these five points for images $[363:383]_{10}$, which we have extracted using the software package GIMP [14].

We first establish how do vertical distances between fixed objects L_1, H_1 and H_2 vary in time. For that purpose we construct two data sets, $DY_{1,2} = Y(L_1) - Y(H_{1,2})$, which we fit to

$$DY_{1,2}(t) = k_{1,2} \cdot (t_{inf} - t). \tag{1.9}$$

We remark that since two distances satisfy Eq. (1.9), throughout the zoom-out the ratio of the distances is fixed,

$$\frac{DY_1}{DY_2}(t) = \frac{k_1}{k_2}, \text{ not a function of time,} \tag{1.10}$$

so either can be used for measuring all the other distances. From the data in Tbl. II, which is plotted in Fig. 4, we find $k_1 = 7.8 \pm 0.2$ s^{-1}, $k_2 = 22.3 \pm 0.5$ s^{-1}, and $t_{inf} = 6.5 \pm 0.1$ s. The metric function thus reads $\mu_{363}(t) = 1p_{363} \times (1 - t/t_{inf})^{-1}$. From [15], p.1-4, we find that the height of the Lunar Module Ascent Stage at the top of the Descent Stage is 2.83 m. From the image 363_{10} we find this distance to be 70 pixels, so $1p_{363} = 4.0$ cm. This allows us to find the liftoff curve, which we provide in Tbl. III and plot as black circles in Fig. 5.

1.3. Results and Discussion

We find the best-fit parameter estimates using the least-squares method. For the S/J Model (1.7) we find:

$$\begin{aligned} \hat{t}_0 &= 0 \text{ s}, \\ \hat{t}_1 &= 0.29 \pm 0.07 \text{ s}, \\ \hat{j} &= 104 \pm 35 \text{ m} \cdot \text{s}^{-3}, \\ \hat{s} &= -673 \pm 385 \text{ m} \cdot \text{s}^{-4}. \end{aligned} \tag{1.11}$$

As can be seen from Fig. 5, the S/J Model (position in red, acceleration in orange) fits the liftoff curve quite nicely over the entire data range.

We extract the parameters of the constant acceleration motion, Eq. (1.8), where we set $t_1 \equiv 0.3$ s,

as

$$\begin{aligned} \hat{a}_1 &= 2.00 \pm 0.50 \text{ m} \cdot \text{s}^{-2}, \\ \hat{v}_1 &= 1.03 \pm 0.60 \text{ m/s}, \\ \hat{x}_1 &= -0.15 \pm 0.33 \text{ m}, \end{aligned} \tag{1.12}$$

where $x(t) = \frac{1}{2}\hat{a}_1\, t^2 + \hat{v}_1\, t + \hat{x}_1$, that is, without offset by t_1. The acceleration $\hat{a}_1$ is in excellent agreement with the expected $a_{max} = 1.95$ m·s^{-2}. For reference we plot Eq. (1.6) in Fig. 5, with position in pink and acceleration in magenta.

As discussed earlier, the warm-up time of the rocket engine (first warm-up time) ended by the time $t = 0$ when the AS started to move. However, the S/J Model suggests that during the second warm-up time, from 0 to $t_1 \simeq 0.3$ s, the Ascent Stage was under influence of a very strong force, which subsequently vanished. This force was responsible for the long-term velocity $\hat{v}_1 \simeq 1$ m·s^{-1}. Because the strong force vanishes after t_1, the J-Model cannot appropriately describe the motion under its influence.

We argue that the long-term velocity $\hat{v}_1$ is not an artifact of improperly compensated zoom-out, but the true feature of the liftoff. To see that, one must recall that zoom-out shrinks the distances in a non-linear fashion, so that the velocity and acceleration are modified, and not just the velocity,

$$x(t) = 1\text{p}_{363} \cdot \frac{DY(t)}{1 - \frac{t}{t_{inf}}} \simeq 1\text{p}_{363} \cdot DY(t) \cdot \left(1 + \frac{t}{t_{inf}} - \frac{t^2}{2\, t_{inf}^2}\right). \tag{1.13}$$

As we find acceleration from the converted liftoff curve to be exactly what we expected, we conclude that the non-zero velocity is not an artifact of conversion, but a feature of the liftoff.

The short burst of force is consistent with an explosion, which produces peak thrust of $F_a \simeq 27$ kN some ~ 0.15 s after the LMAS starts to ascend. For comparison, the rocket engine produces thrust $F_{th} = 2.2 \cdot m_0^{AS}\, g \simeq 16$ kN. Here, we remark that the crew used explosive devices in preparation for liftoff to separate the electrical and mechanical connections between the stages, and to vent the DS fuel tanks so they would not ignite during liftoff. These devices, however, would be activated in preparation for ascent- not after the Ascent Propulsion System was started. Coincidentally, the frames 365_{10} (+0.2 s) onward, in Fig. 3, suggest a visible explosion taking place between the Ascent and the Descent Stage as they separate: The amount of flying debris and its brightness is maximal in the frame 366_{10} (+0.3 s) and subsides thereafter. On the `ApolloHoax.net` discussion thread [16] it was proposed that the visible explosion provided additional propulsion through the Jules Verne's "bullet in the barell" launching method. This argument is flawed, as the

rocket engine immediately blows dust from the surface, making build-up of exhaust gas pressure unlikely anywhere in the Descent Stage (DS). In addition, the empty volume in which the nozzle sits in the DS that could potentially serve this purpose is not in any way structurally reinforced to sustain such pressures. It is also rectangular in shape which directs gas flow toward the edges, making them fall apart (and so let the gas inside the DS).

The explosion appears to be an unplanned event, thus its direction and magnitude must be random. Asymmetry of the explosion would destabilize the vessel, appearing as forced change in roll or pitch angle or rate. It is established that the rocket is marginally stable with respect to small changes in roll or pitch angle φ; unless counteracted by the Abort Guidance Section (AGS) [17] the roll or pitch motion introduced by the explosion would continue unhindered. The lateral acceleration of the vessel would then become:

$$\ddot{y} = \sin\varphi \cdot \frac{F_{th}}{m}. \tag{1.14}$$

For example, 1^o un-compensated pitch for a duration of 2 seconds causes the vessel to move laterally by $y \approx 12$ cm, and to continue drifting at $\dot{y} \approx 12$ cm/s. This lateral motion would be easily visible on the video recording with its ~ 4 cm/pixel resolution. We remark that the AGS cannot counteract such minute lateral motion because it is below its detection thresholds. It is also unnecessary considering its goal of meeting with the Control and Service Module (CSM) in lunar orbit.

1.4. Tables and Figures

Name	Quantity	Value
Lunar gravity	g	1.622 m·s^{-2}
Ascent Stage height	l_{AS}	3.76 m
Descent Stage height	l_{DS}	3.23 m[a]
Ascent Stage mass (dry)	m_d^{AS}	2132 kg
Ascent Stage propellent mass	m_p^{AS}	2359 kg
Ascent Stage total mass	m_0^{AS}	4491 kg
Descent Stage mass (dry)	m_d^{DS}	2767 kg
Lunar Module Earth Launch	m^{LM}	16375 kg
Landing Mass	$m_{LM} \approx m_0^{AS} + m_d^{DS}$	7258 kg
APS Thrust	F_{th}	16,000 N
Propellent expelled velocity	w	3050 m/s
APS Thrust-to-Weight at Liftoff	$\alpha = F_{th}/(m_0^{AS} \cdot g)$	2.20

[a]This assumes un-deployed primary struts. See discussion in the text.

TABLE I: Relevant Lunar Module Data for Analysis of Liftoff. [7, 8]

Image No.	$Y(H_1)$	$Y(H_2)$	$Y(L_1)$	$Y(M_1)$	$Y(M_2)$
363	296	246	150	236	271
364	295	245	150	234	268
365	294	244	151	233	265
366	291	243	152	229	263
367	290	243	153	224	254
368	289	241	153	220	249
369	286	239	154	212	243
370	284	239	155	208	236
371	282	238	155	200	230
372	280	237	156	194	224
373	278	235	156	187	217
374	277	234	156	183	210
375	275	234	158	175	203
376	274	233	158	168	197
377	272	231	158	162	189
378	272	231	159	155	182
379	269	230	160	148	174
380	267	230	160	142	168
381	267	228	160	133	159
382	264	227	161	127	153
383	264	227	161	120	145

TABLE II: Pixel Y-coordinates of the reference points on the Lunar Module and the Moon landscape in the images $[363 : 383]_{10}$. The reference points are shown in Fig. 2, while the images are combined in Fig. 3.

Time (s)	Ascent (m)
0.0	0.00
0.1	0.08
0.2	0.12
0.3	0.20
0.4	0.42
0.5	0.59
0.6	0.87
0.7	1.02
0.8	1.35
0.9	1.61
1.0	1.92
1.1	2.14
1.2	2.53
1.3	2.92
1.4	3.23
1.5	3.71
1.6	4.05
1.7	4.40
1.8	5.05
1.9	5.38
2.0	5.96

TABLE III: First two seconds of liftoff of the Apollo 17 Lunar Module Ascent Stage.

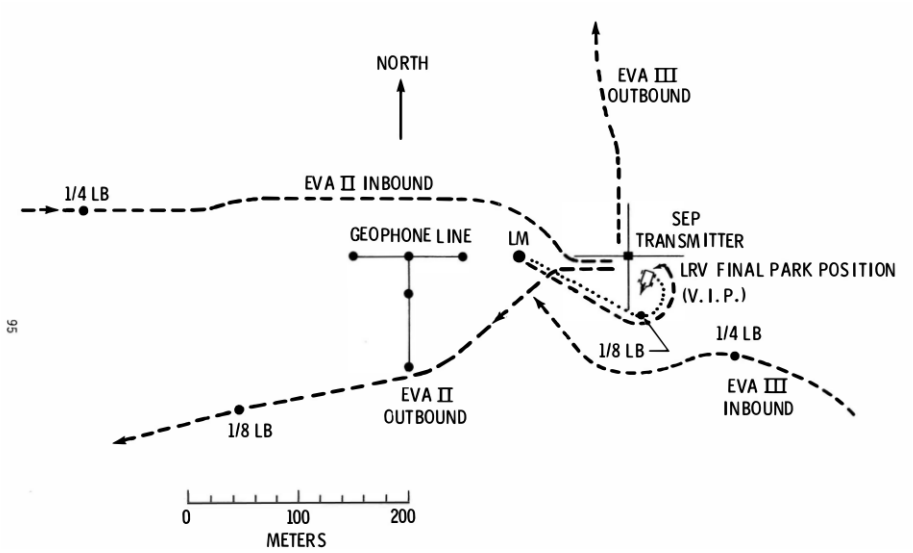

FIG. 1: The map of the Apollo 17 landing site on the Moon [1] shows the location of the Lunar Roving Vehicle (LVR), which carried the remote-controlled camera that recorded the liftoff.

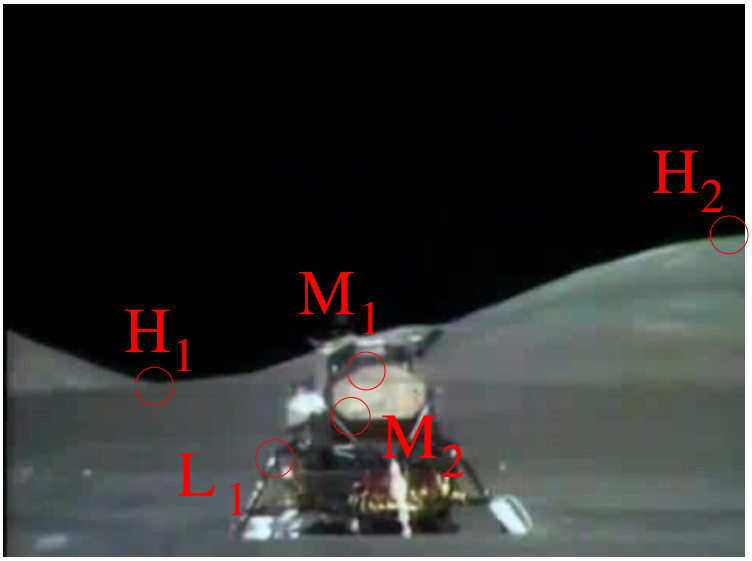

FIG. 2: The reference points on the Lunar Module and the Moon landscape in the image 363_{10} that are used for extraction of liftoff curve.

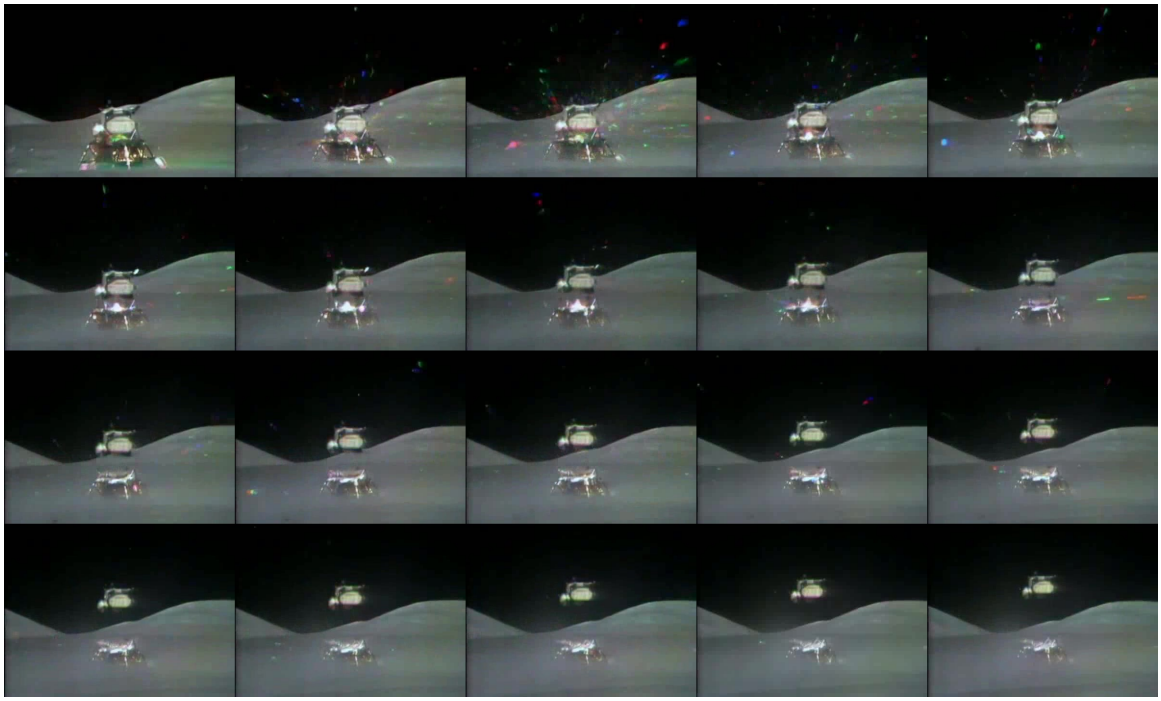

FIG. 3: Composition of the images $[364 : 383]_{10}$, which are used for extraction of Y-pixel positions of the reference points. The image numbers go left-to-right, top-to-bottom, and are spaced at 0.1 second interval. The extracted positions are given in Tbl. II.

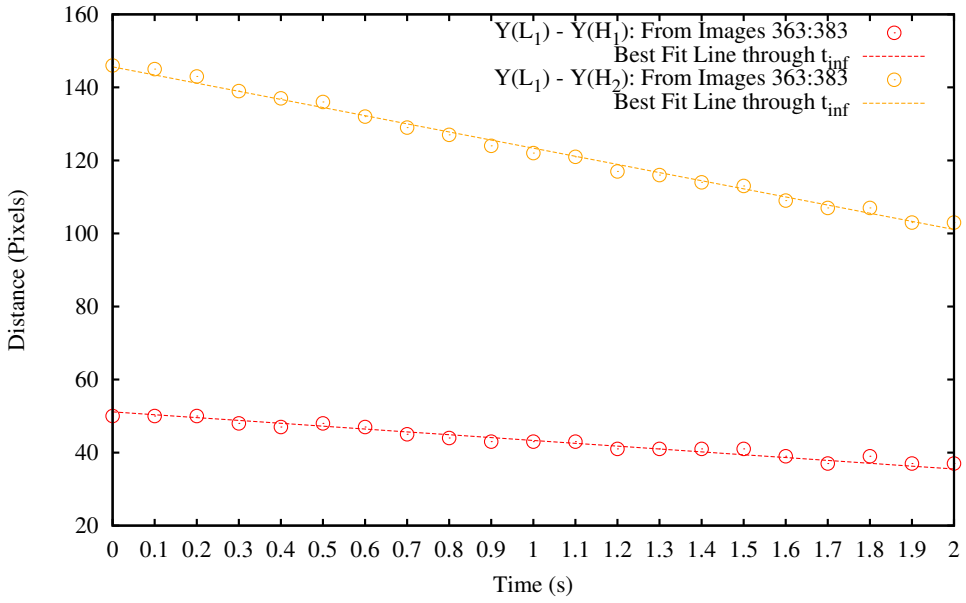

FIG. 4: Vertical distance in pixels between the reference points in images $[363 : 383]_{10}$ with the best-fit linear models used for removal of camera zoom-out.

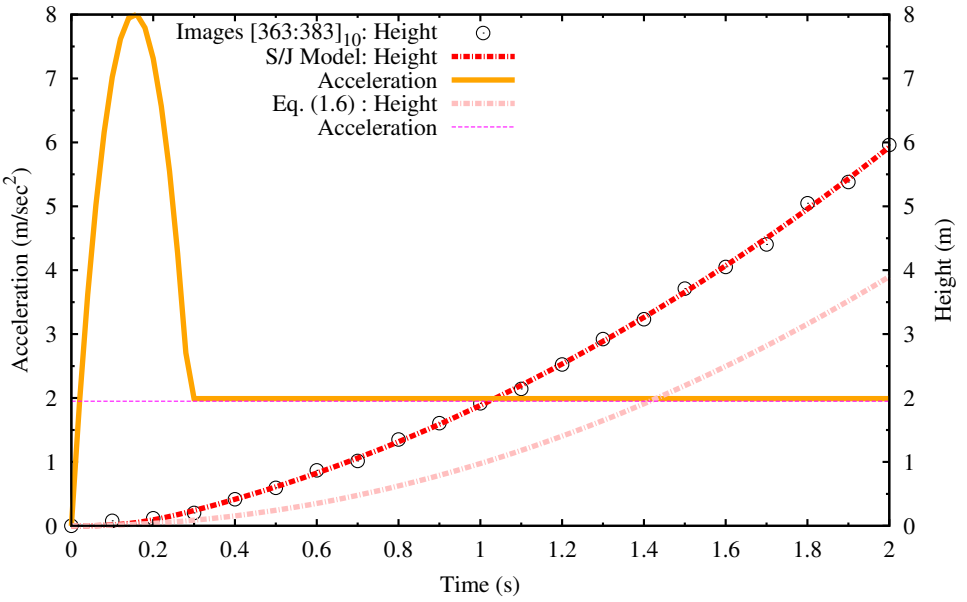

FIG. 5: Apollo 17 Lunar Module Ascent Stage liftoff curve from Tbl. III (black circles), does not match the constant acceleration motion starting from rest (position in pink, acceleration in magenta) given by Eq. (1.6) except in the acceleration of the ascent. The S/J model (position in red, acceleration in orange) besides fitting the liftoff curve well, also suggests an explosion taking place in the first 0.3 seconds of liftoff, which gives the Ascent Stage extra velocity of $v_0 \simeq 1$ m/s.

2. AND SHAKE A LEG, SHAKE A LEG, SHAKE A LEG, SHAKE IT AGAIN

We focus next on deployment of primary struts in Apollo 11 and 17 missions.

As shown in Fig. 6, the primary strut (PS) is the crucial element of the landing gear. Its purpose is to attenuate the impact of landing on the lunar surface. The strut is a piston-cylinder type; it absorbs the compression load of the lunar landing and supports the Lunar Module (LM) on the lunar surface. Compression loads are attenuated by a crushable aluminum-honeycomb cartridge in each strut. [7] The primary strut shortens as a result of deployment.

In this section, we derive the maximal stress the primary struts were designed to handle, and how much they would shorten if the landing were soft or standard. We then examine the images of landing gear and establish whether the primary struts shortened as expected, and by how much.

2.1. Physical Model of Primary Strut and its Performance Parameters

We first consider landing against hard (immobile) surface. The maximum compression (deployment) length of the strut is by design $l_{max} = 0.81$ m. They struts come at an angle of $\varphi = 30^o$ with respect to the vertical X-axis, so the vertical distance they can travel is $x_{max} = l_{max} \cos\varphi = 0.70$ m. By design, the primary strut can absorb at most $v_{max} = 3.0$ m/s vertical impact velocity in the absence of horizontal motion. This corresponds to free fall from $h_{max} = 2.8$ m. The crushing of aluminum-honeycomb elements of the primary struts act as an unidirectional friction force F_{PS}. From energy considerations and the LM data from Tbl. I, we know

$$\frac{m_{LM}}{2}\, v_{max}^2 + m_{LM}\, g\, x_{max} = F_{PS}\, x_{max}, \tag{2.1}$$

so

$$F_{PS} = 60 \text{ kN}, \tag{2.2}$$

We next examine what stress the landing gear and the primary struts undergo as a function of impact velocity. We condider two cases that have appeared in the literature:

1. **Charmin®Ultra Soft^{TM} Landing**:

   According to [18], upon reaching the landing point with nulled horizontal velocity, the LM would descend to the lunar surface with $v_l = 0.91$ m/s sink rate. This v_l is equivalent to free

fall from the distance,

$$h_l = \frac{v_l^2}{2\,g} = 25 \text{ cm}, \tag{2.3}$$

at which the Descent Propulsion System (DPS) would be turned off. We remark that the Reactive Propulsion System (RPS) cannot be used to maintain sink rate instead of the DPS because (i), RPS does not have enough thrust to counteract the weight of the LM, and (ii), the exits of the RPS jets in the direction of the ground point to heat shields on the Descent Stage, which deflect exhaust gases by 90^o away from the DS. The latter makes the jets less efficient for vertical propulsion, while also providing undetermined horizontal drift to the LM.

Assuming that v_l is the surface impact velocity, the primary struts are deployed by

$$\Delta X = \frac{x_{max}}{h_{max}}\, h_l = 6.3 \text{ cm (vertically), or } \Delta l = 7.3 \text{ cm (along the strut).} \tag{2.4}$$

2. **Standard Landing**:

   The LM features three Lunar Surface Sensing Probes, stretching $h' = 1.71$ m (5'7.2") below the Left, Right and Aft footpad. Their role was to alert the crew to proximity of lunar surface, prompting them to turn off the DPS. The free fall from the height h' ends in the impact velocity of

$$v_l' = \sqrt{2\,h'\,g} = 2.3 \text{ m/s}, \tag{2.5}$$

   so the deployment distance is

$$\Delta X' = 43 \text{ cm (vertically), or } \Delta l' = 49 \text{ cm (along the strut).} \tag{2.6}$$

The interaction between the rocket engine and the lunar soil would determine the condition of two elements of the LM undercarriage: the radiation shield (a few-microns thick gold foil around the bottom of the Descent Stage), and the protective shrink wrapping (Kapton and mylar) of the landing gear. The images of the Apollo 11 landing site are consistent with the *bearing failure* theory that was developed around the time of the Apollo programme. According to this theory, lunar sand flows down and perpendicularly outwards from the rocket jet to make a wide and shallow indentation in the soil, so the sand never reaches the LM undercarriage. The pristine Apollo 11

undercarriage and the miniscule congregation of dust on the landing gear and inside the footpads all support the theory, as the images AS11-40-5921 [19, 20] or AS11-40-5927 [19, 21] demonstrate. However, Metzger *et al.* [22] have shown that this theory is innacurate: When operating close to a sandy surface, the rocket jet digs a hole of comparable diameter along the sides of which the sand flows tangentially upwards. The amount of sand excavated from the hole at high velocity would sand blasted the undercarriage clean of any shrink wrapping and leave copious abrasion marks dispersed across the LM underside. In addition to this inconsistency, the image AS11-40-5921 also suggests that the Apollo 11 LM underwent an impossible landing sequence. To land softly the LM needs the DPS to operate to very low heights, but the image shows that the right Lunar Surface Sensing Probe (LSSP) digs a trench in the sand that stretches from under the rocket engine to its final resting position. The substrate of the landing surface must be sand because the LSSPs cannot dig trenches in firm soil or stone. Additonally, the trench that was just dug in the sand (its depth, edges, length and position) would be wiped out by the sand moved by a functional rocket jet operating nearby. The jet could not be off, however, because the LM did hover to its final landing position without loss in height (as attested by the decreasing depth of the trench as the LSSP is approaching its final landing position).

This digression not-withstanding, we determine how deep the footpads penetrate the lunar sand, where we model the resistance to penetration in two ways:

1. **Flat-foot Approximation**

   We split the Lunar Module (LM) into two masses, m_2 of landing gear, and m_1 of the rest with $m_1 \gg m_2$, where the two are at positions x_2 and x_1, respectively. This is shown in Fig. 7. Their motion is described by a system,

$$\begin{aligned} m_1\,\ddot{x}_1 &= m_1\,g - T_{PS}, \\ m_2\,\ddot{x}_2 &= m_2\,g + T_{PS} - R_{moon}, \end{aligned} \tag{2.7}$$

   where R_{moon} is the resistance of the Moon surface to penetration. It is not difficult to see that for the primary strut to shorten during penetration ($T_{PS} \equiv F_{PS}$), the force to penetration in the lunar sand has to satisfy,

$$R_{moon} > F_{PS} \cdot \left(1 + \frac{m_2}{m_1}\right), \tag{2.8}$$

   or otherwise the LM sinks.

   Assuming this indeed to be the case, it is not difficult to see that the solutions to Eq. (2.7)

are,

$$\begin{aligned} \dot{x}_1 &= v_0 - a_1\, t, \text{ for } 0 \le t \le \tfrac{v_0}{a_1}, \text{ and} \\ \dot{x}_2 &= v_0 - a_2\, t, \text{ for } 0 \le t \le \tfrac{v_0}{a_2}. \text{ where} \\ a_1 &= \tfrac{F_{PS}}{m_1} - g, \text{ and} \\ a_2 &= \tfrac{R_{moon} - F_{PS}}{m_2} - g. \end{aligned} \tag{2.9}$$

Here, $v_0 = \dot{x}_1(0) = \dot{x}_2(0)$ is the impact velocity at the surface, while $a_2 > a_1$, which is equivalent to Eq. (2.8), assures the deployment of the landing gear.

The displacements we are interested in are,

$$\begin{aligned} x_2 &= \tfrac{m_2\, v_0^2}{2\,(R_{moon} - F_{PS} - m_2\, g)}, \text{ for penetration in the Moon soil, and} \\ \Delta x &= \tfrac{v_0^2}{2\, a_2} - \tfrac{v_0^2}{2\, a_1}, \text{ for shortening of the strut.} \end{aligned} \tag{2.10}$$

The limit $m_2 \to 0$ and $R_{moon} \to \infty$ is equivalent to the immovable hard surface, where $x_2 = 0$ and $\Delta x = m_1\, v_0^2/(2 \cdot (F_{PS} - m_1\, g)) = \Delta X, \Delta X'$, depending on the landing roughness. Consider a more realistic estimate, in which the landing gear has mass $m_1 = 500$ kg, while the rest is $m_2 = 6758$ kg, and $R_{moon} = 300$ kN. Under standard landing conditions $h' \sim 1.7$ m, we find $x_2 = 0.5$ cm for penetration and $x_2 - x_1 \simeq 43$ cm for shortening of the primary strut. We conclude that in the Flat-foot approximation under realistic landing conditions, the penetration in the Moon, and the shortening of the primary strut are well described as if the surface of the Moon were impenetrable.

2. **Round-foot Approximation**

The actual footpads are not flat but round more like spherical caps. We find that the radius of the sphere is $r = 1.5$ m, while the depth of the cap is $d = 7$ cm. Then, as the footpad penetrates the lunar sand by depth x_2, its contact surface S_{foot} varies as

$$S_{foot} = 2\,\pi\, r\, x_2. \tag{2.11}$$

The resistance of the Moon surface to penetration by a quadruped can then be described

$$R_{moon} = 4 \times P_{moon} \cdot S_{foot} = 8\,\pi\, r\, P_{moon}\, x_2, \tag{2.12}$$

where we assume that the resistance pressure $P_{moon} \approx$ const.

We estimate P_{moon} from pictures of astronauts hoping on the Moon: We assume that a 300 cm^2 foot of a 150 kg astronaut penetrates the Moon by 1 cm in fall from 10 cm height, which yields $P_{moon} \sim 90,000$ Pa. This allows us to express $R_{moon} = k_{moon} \cdot x_2$, where

$$k_{moon} = 3.4 \cdot 10^6 \text{ N/m}, \tag{2.13}$$

and $\omega = \sqrt{\frac{k_{moon}}{m^{LM}}} = 21 \text{ s}^{-1}$. From the energy conservation, we can estimate the penetration x_2' in the lunar sand by a footpad,

$$\frac{k}{2} x_2'^2 - F_{PS}\, x_2' \simeq \frac{m_2}{2} \dot{x}_2^2(0), \tag{2.14}$$

where we neglect the gravity acting on the footpad because $m_2 \cdot g \ll F_{PS}$. The solution of Eq. (2.14) is

$$x_2' \simeq \frac{F_{PS}}{k_{moon}} + \sqrt{\left(\frac{F_{PS}}{k_{moon}}\right)^2 + \frac{m_2}{m^{LM}} \left(\frac{v_0}{\omega}\right)^2} \geq 2\, \frac{F_{PS}}{k_{moon}} = 3.6 \text{ cm}. \tag{2.15}$$

In this estimate the second term under the square-root begins to dominate for greater impact velocities. E.g., for standard landing with $m_2/m^{LM} \sim 0.1$ and $v_0 \equiv v_l' \simeq 2.3$ m·s^{-1} we find this term to be 3.6 cm, so then $x_2' \simeq 5.7$ cm.

To estimate the shortening of the struts we start with the Flat-foot approximation. Here we know that for as long as Eq. (2.8) is not satisfied, the footpad penetrates the Moon without deployment of the primary strut. We find this distance x_2'' to be

$$x_2'' = \frac{F_{PS}}{k_{moon}} \left(1 + \frac{m_2}{m_1}\right) \simeq \frac{F_{PS}}{k_{moon}} = 1.8 \text{ cm}. \tag{2.16}$$

Following x_2'' the initial velocity of the Lunar Module v_0 drops to

$$v_1 = \sqrt{v_0^2 + 2\, g\, x_2'' - \omega^2\, x_2''^2}. \tag{2.17}$$

At this point, we can drop the linear model of the resistance to penetration and revert to the impenetrable surface limit. In this limit we find that for soft landing and $v_0 \equiv v_l = 0.91$ m/s the deployment of the primary struts is $\Delta X = 5.1$ cm, while for standard landing and $v_0 \equiv v_l' \simeq 2.3$ m/s we find $\Delta X' \simeq 41$ cm.

Overall, we can summarize the analysis as follows. The Round-foot approximation allows us to estimate how much the footpads penetrate the lunar surface during landing,

$$x_2' \gtrsim 3.6 \text{ cm}, \tag{2.18}$$

irrespective of impact velocity. For comparison, the footpad is $d = 7$ cm deep. The Flat-foot approximation provides us with an approximate deployment distance of the primary strut during landing,

$$\Delta l = \text{between 7 and 49 cm}, \tag{2.19}$$

which strongly depends on the impact velocity.

2.2. Results and Discussion

Method: We use the fact that Fig. 6 is drawn to scale. As a measuring stick we use the diameter of the footpad $D_t = 0.93$ m. The most useful is the distance between the lower side of the secondary strut connection, and the footpad joint, call it l_{PS}, which is also equal to D_t. The analysis of images thus represents comparing the diameter of the footpad D_t to the length l_{PS}.

For the Apollo 11 LM on the Moon we use the images in Fig. 8, while in space we use the images AS11-44-6584 (for aft and front footpad and their primary struts) and AS11-44-6577 (for left and right footpad and their primary struts) provided in Fig. 16. In all cases we find that this ratio is unity, and conclude that during landing on the Moon the Apollo 11 primary struts were undeployed. The same images also show that neither of the footpads penetrates the Moon surface to any appreciable depth.

Overall, the (lack of) deployment of landing gear suggests that the landing was softer then even the *Charmin*® *Ultra Soft*^{TM} landing: Here, the Descent Propulsion System must be active until the footpads touch the Moon surface. For landing on the Moon this is impossible because of at least two reasons:

1. The LM crew did not have a device to precisely measure the distance from the ground for the purpose of landing, except for the Lunar Surface Sensing Probes (LSSP), which extended ~ 1.7 m below the footpads.

2. The LM undercarriage is in pristine condition indicating no sandblasting has ever taken

place, but this is inconsistent with firing of a rocket jet close to the sandy surface that softer then *Charmin®Ultra Soft*^{TM} landing requires.

On the contrary, what we see is consistent with the public perception of the Apollo 11 landing that it was staged somewhere on the Earth, with either a replica or the spare LM, which was lowered to the ground with a crane. For staging the landing on the Earth, it is necessary to do it softly to avoid deployment of the primary struts. Their $F_{PS} \simeq 60$ kN is sufficient to hold the LM total dry weight of ~ 48 kN without deploying only if the impact velocity is minimal.

Considering all the forces acting on the Descent Stage (DS), rigidity of the landing gear in the video recording of the Apollo 17 liftoff is just as dubious. For example, in the initial moments of liftoff the exhaust gases pushed the DS downwards with the same thrust F_{th} that propelled the AS upwards (3^{rd} Newton Law). As the thrust of the AS engine is much greater then the weight of the dry DS ($F_{th}/(m_d^{DS}\, g) \gtrsim 3$), and considering that the DS should be somewhat flexible, we would have expected the DS to visibly shake in the initial moments of ascent. It does not, and it is doing it so well that we used the top of the primary strut as one of the reference points for measuring distances. The explosion shortly after liftoff should further perturb the DS. Conspicuous absence of any DS motion suggests that we are looking at a scaled-down liftoff featuring detailed models. We further develop this idea in the next section.

2.3. Tables and Figures

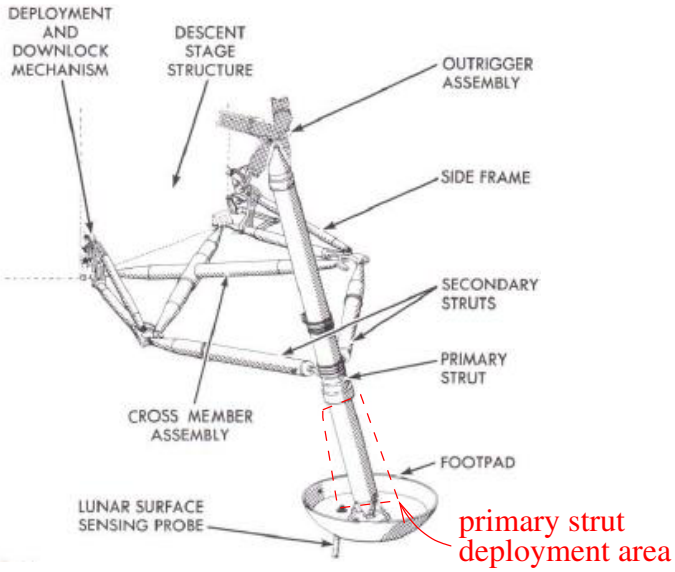

FIG. 6: Landing gear assembly from [15] features un-deployed primary strut, where the deployment area is marked in red. The magnitude of deployment (shortening of the primary strut) is discussed in the text as a function of landing roughness.

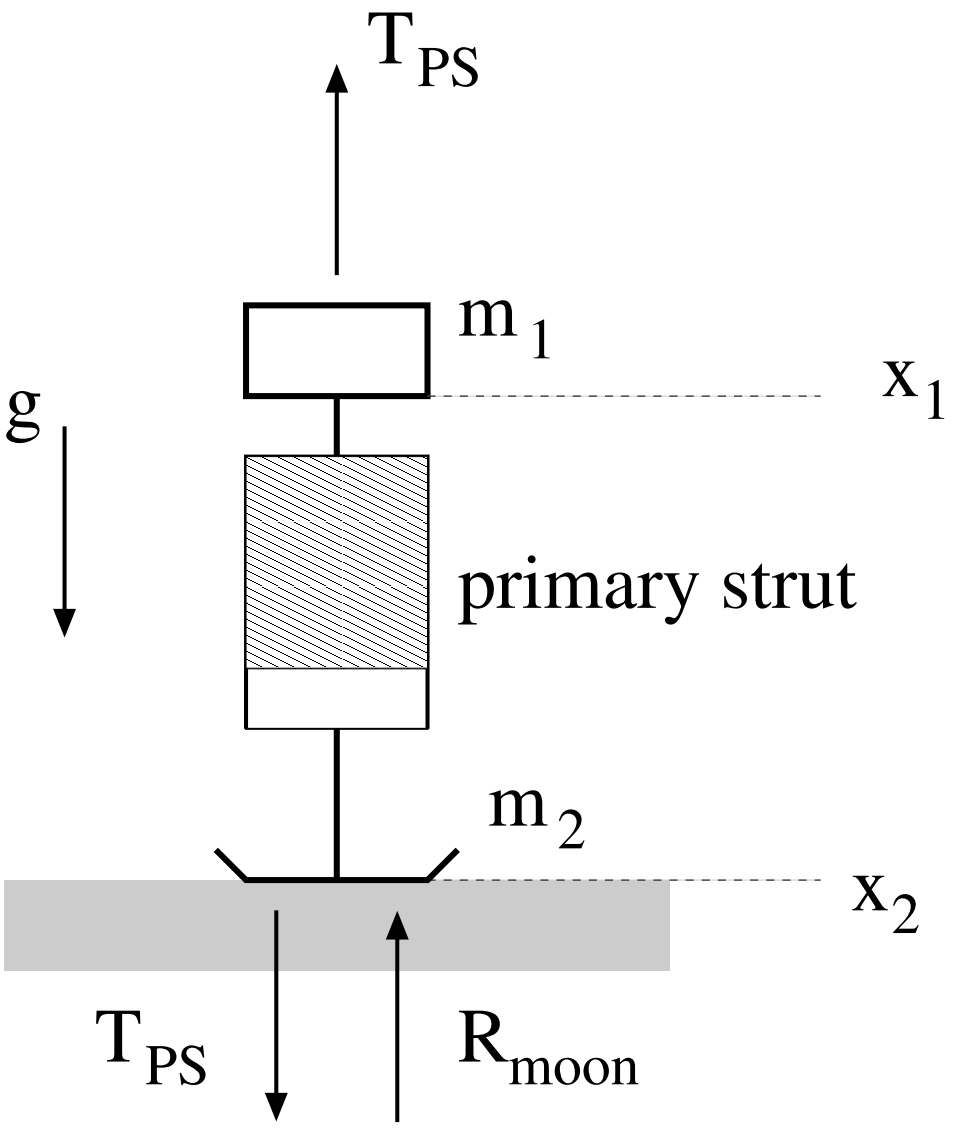

FIG. 7: Physical model of deployment of the primary strut in impact with the soft surface described by the resistive force R_{moon}, while T_{PS} is the primary strut tension. The Lunar Module is conveniently split in two masses, m_2 of the struts and footpads, and m_1 of everything else. See discussion in text.

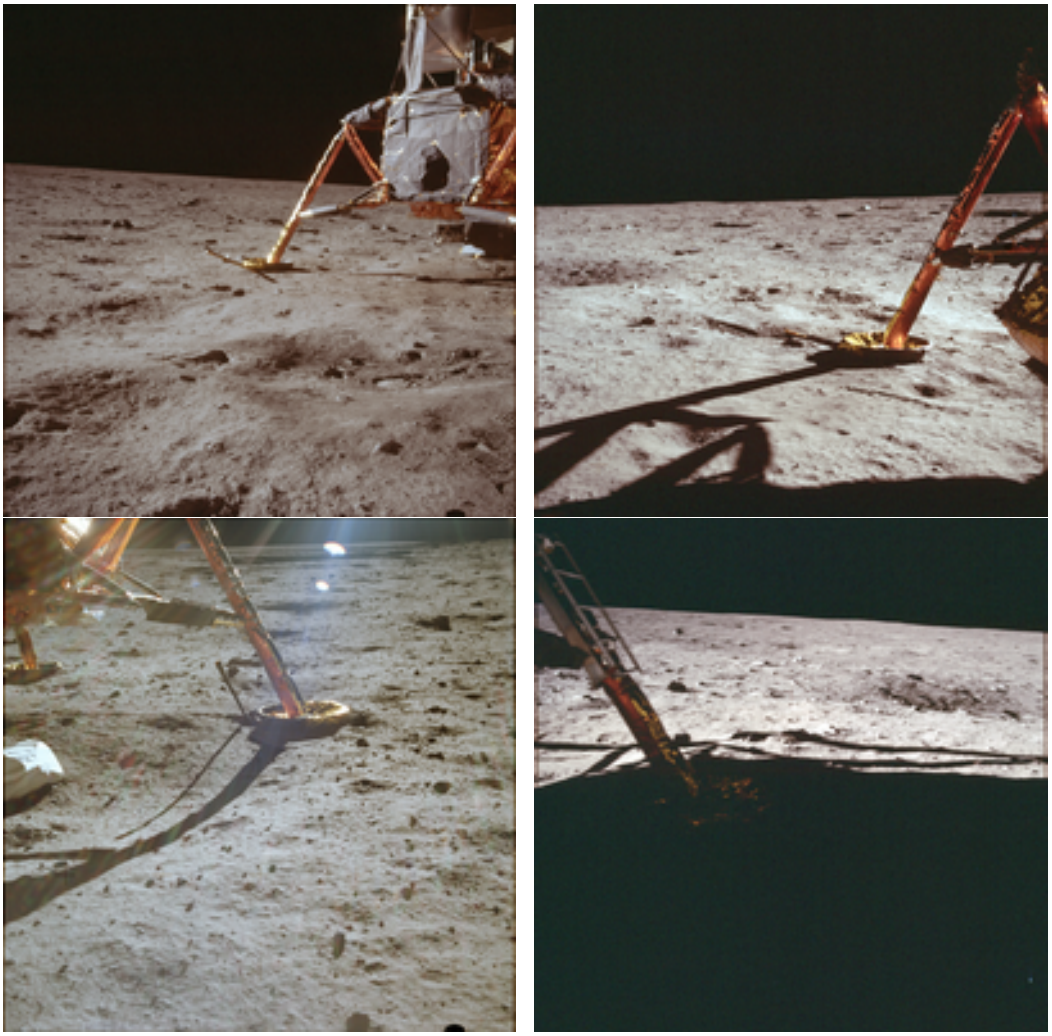

FIG. 8: Images of the landing gear of the Apollo 11 Lunar Module (LM) feature un-deployed primary struts after landing on the Moon (top left, AS11-40-5914, aft gear; top right, AS11-40-5858, left gear; bottom left, AS11-40-5865, right gear; bottom right AS11-40-5859, front gear). The same gear in space prior to the Descent-Orbit-Insertion for the Moon landing is shown in Figs. 16 and 17. In both groups of images for each landing gear one compares the diameter of the footpad to the distance between the secondary strut attachment point and the footpad joint on the primary strut. Also notice that on the Moon the footpads do not penetrate the Moon soil. See discussion in the text for the anticipated performance of the landing gear.

3. ALSO SPRACH ZARATHUSTRA

We return to the Apollo 17 lift-off video recording [10] and analyze it in greater detail following the findings of last two sections. For the purposes of our analysis we convert the video clip to a set of images at rate $r = 25$ frames-per-second (fps) [52]. We firstly analyze the images $[681 : 901]_{25}$ featuring stationary Lunar Module (LM) prior to the lift-off. Then we examine size and illuminance of the ascending LM in the images $[981 : 1012]_{25}$.

3.1. Film Stock

Method: We examine frames $[681 : 901]_{25}$ using the software package GIMP [14], at various brightness and contrast settings.

Findings: In the frames $[681 : 685]_{25}$ under the extreme settings of 127 for brightness, and 127 for contrast we find identical artifacts that strongly resemble an edge of film stock. We show the frame 681_{25} in Fig. 9 in which the artifact stretching horizontally across the image is obvious. Presence of the film stock is surprising, considering that NASA claims that this video was recorded by a television camera. [3]

3.2. Flicker

Following an examination of video recording with the software package `ffmpeg`, it transpires that it was recorded at the 25 fps. During the watching the video recording appears to be flickering.

Method: For each image in the sequence $[681 : 901]_{25}$ we determine the average values for red, green and blue channel. [23] From the averages we create three 221-samples long time series $\{R_{680+i}, G_{680+i}, B_{680+i}\}_{i=1,221}$. We regularize each series with its total average $\bar{R}$, $\bar{G}$, $\bar{B}$, so $a_i = A_i/\bar{A} - 1$, for $\{a, A\} = \{\{r, R\}, \{g, G\}, \{b, B\}\}$. We then split regularized time series to 128-samples long sequences, which we Fourier Transform, and then average so found modulation depths.

Findings: As can be seen from Fig. 10 there is light flicker in the video recording, which frequencies are 5 Hz and 10 Hz, where the red and green peaks are stronger at 5 Hz then at 10 Hz, while the blue is the opposite.

Discussion: As is known, one way of creating 5 Hz flicker consists of using a film camera that records at 25 fps, while the illumination is provided by incandescent lamps (have strong red component) operating at 60 Hz, so its light output is modulated at 120 Hz, which is twice the mains frequency. More precisely, 120 Hz signal when sampled at 25 Hz becomes 5 Hz because of

aliasing. Because of the non-linear characteristic of incandescent lamps, where their light output is proportional to input power and the temperature of the filament, the light may contain second and higher harmonics, hence the 10 Hz peak. The modulation depth of the recorded light is in the range $\sim 1\%$ (blue) to $\sim 3\%$ (red), which is lower then the actual modulation depth of the incandescent lamps ($\gtrsim 10\%$) because the camera exposure time acts as an integrator (low-pass filter).
We isolate the 5 Hz changes in the lighting patterns using GIMP [14], where we set brightness to 50 and contrast to 127. In Fig. 11 we show a 6-frame sequence $[681 : 685]_{25}$, and there the lighting pattern can be recognized (i), in the lower right corner with respect to the Lunar Module (ground on the right from the LM); and (ii), on the hill on the right (which is presumable far) behind the LM. The two lighting patters are consistent with the LM being side- and back- illuminated with incandescent lamps in-phase (from the same source). However, that the illumination of the entire hill (presumably Camelot) is uniformly modulated suggests that the hill is a two-dimensional image of a geographical feature close to the LM, rather than a spatially extended feature stretching far behind the LM.

3.3. Space Rocket or Space Elevator?

We look at the images $[981 : 1012]_{25}$ depicting the last 1.3 s of the ascent, after which the camera view changes to inside view. In Tbl. IV we list the positions of bottom left corner of the LMAS in each image, where the x direction is horizontal, while y direction is vertical. We note that the camera almost perfectly follows the LMAS.

It has been proposed many times in public media that the video features the LMAS replica being pulled up in, what we call, the space elevator, rather then the real LMAS being propelled by its own space rocket. The two propulsion mechanisms, space rocket vs. space elevator, have different center-of-pressure: For rocket powered LMAS, the center-of-pressure is the exit of combustion chamber (at the bottom if we neglect the nozzle), while for hoisted replica, the center-of-pressure is the attachment point to the elevator (top of the object). It is important to recognize that two propulsions react differently to perturbations, where the perturbations are most pronounced opposite the center-of-pressure. The real LMAS is marginally stable with respect to changes in roll or pitch angles, so the real LMAS moving upwards may also drift sideways.
The replica pulled up can be described as a simple gravity pendulum of arm length l_{CM}, in an accelerating space elevator with the acceleration $a_e \approx$ const. It performs harmonic motion with the frequency of small oscillations $\omega = \sqrt{(a_e + g)/l_{CM}}$.

We depict the distinction between two propulsion mechanisms in Fig. 12.

The video recording features few swings of the bottom of the object, of which one half-period can be clearly identified in images $[994:997]_{25}$. Its duration is $\sim 3/25 = 0.12$ s, while its appearance suggests under-damped motion of period,

$$T_{v:a17} \gtrsim 0.3 \text{ s}, \tag{3.1}$$

and frequency $f_{v:a17} \sim 4$ Hz. A true-to-life replica being hoisted up somewhere on the Earth would have oscillated with a period

$$T_{AS} > 2\,\pi \sqrt{\frac{l_{CM}}{g_{Earth}}} = 3.1 \text{ s}, \tag{3.2}$$

where $l_{CM} = 2.4$ m is the center-of-mass distance from the center-of-pressure. We find $T_{AS} \gg T_{v:a17}$, so the featured object is not true-to-life replica. However, if this were a 1:48 scale model, then its period would be $T_{AS} \sim 2.4/\sqrt{48} \sim 0.45$ s, which is of the same order of magnitude as $T_{v:a17}$.

3.4. Heading for the Light

One may argue that the object motion cannot be detected with certainty because of the poor resolution of the images. Were we able to see specular reflection of the Sun from the object surface this would have increased our chances to detect micro-motion - we would just have to look for modulations in magnitude of the specular reflection beyond the observed 5 and 10 Hz, provided they not saturate the camera. However, we find no evidence of specular reflection just from the geometry of the scene: the Sun is at least 50^o above horizon behind the camera, while for the duration of video recording analyzed here the object moves from 6^o to 12^o above horizon and does not approach to the Sun's angle.

Rather, we notice that if the video recording is from the Moon then the light comes from the Sun at infinity, so its angle with respect to the object is fixed during lift-off. Then, the average illuminance of the LMAS should be constant for as long as the angle between the LMAS and the Sun, and the angle between the camera and the LMAS are sufficiently different so we do not have specular reflection. Conversely, if the scene is staged scaled down, then the lighting is provided by arrangement of near-by lamps, and the camera might be able to capture systematic changes in illuminance if the object as it ascends approaches to the stage lighting.

We determine the average illuminance of the object as follows. For each image in the sequence $[981:1012]_{25}$ we isolate the segments 61 pixels wide and 46 pixels high, which lower left corner are given in Tbl. IV. In Fig. 13 we combine all analyzed image segments in one composite image. The segments feature the AS, black background and some reflections from the dust. We introduce threshold λ^a, $a = R, G, B$, and in each image segment determine mean pixel value above the threshold λ^a,

$$\bar{c}^{a,k}(\lambda^a) = \frac{1}{\sum_{i,j} \mathcal{H}(c^{a,k}_{i,j} - \lambda^a)} \sum_{i,j} \mathcal{H}(c^{a,k}_{i,j} - \lambda^a) \cdot c^{a,k}_{i,j}, \tag{3.3}$$

where $k = 981 \ldots 1012$, while Heaviside function is $\mathcal{H}(x) = 1$ for $x > 0$, and 0 otherwise. In Fig. 14 (top panel) we can see that the average pixel value $\bar{c}^{a,k}$ for $\lambda^a = 50$, a =R,G,B, increases with image number, that is, as the object gains height.

One possible explanation of this effect is given in Fig. 14 (bottom panel). The object illuminance is a function of the light source altitude θ, as

$$l_\theta = \frac{S \cos\theta}{r_\theta^2}. \tag{3.4}$$

We find how does the relative illuminance changes between two positions, the initial 0 and some later 1, if we assume that the source of light is at distance b from the line along which the object ascends. Then the ratio of illuminances between two positions is,

$$\frac{l_{\theta_1}}{l_{\theta_0}} = \frac{\cos^3\theta_1}{\cos^3\theta_0} \simeq 1 - 3\tan\theta_0 \cdot (\theta_1 - \theta_0) + \ldots. \tag{3.5}$$

We find $\Delta x \cdot \cos\theta_0 = b/\cos\theta_0 \cdot \Delta\theta$, where $\Delta\theta = \theta_1 - \theta_0 \leq 0$ and $\Delta x = x_1 - x_0 \leq 0$. We know that the object moves so $x(t) = \frac{1}{2}\,\hat{a}_1\,t^2 + \hat{v}_1\,t + \hat{x}_1$, so $-\Delta x = \frac{1}{2}\,\hat{a}_1\,\Delta t^2 + (\hat{a}_1\,t_0 + \hat{v}_1)\,\Delta t \propto \Delta t^2 + 2\,(\hat{a}_1\,t_0 + \hat{v}_1)/\hat{a}_1\,\Delta t$. With the timing information from the image sequence, $t_0 = (981 - 902)/25 = 3.2$ s, we find $2\,(\hat{v}_1 + \hat{a}_1\,t_0)/\hat{a}_1 \simeq 7.4$ s, so the theoretical prediction for the change in illumination is,

$$\frac{l_{R,G,B}(\Delta t)}{l_{R,G,B}(t_0)} = k_2\,(\Delta t^2 + 7.4\text{ s}\cdot\Delta t) + k_{R,G,B}. \tag{3.6}$$

From the pixel data we find $k_2 \simeq 0.0092\text{ s}^{-2}$, and $k_{R,G,B} = 0.98$. In Fig. 14 (top panel) we compare the average pixel channels to the best-fit models (3.6), and find an excellent agreement. An upper

limit on the distance b between the light source and the AS trajectory thus reads,

$$b = \frac{3\,\hat{a}_1\,\sin(2\theta_0)}{4\,k_2} \leq \frac{3\cdot\hat{a}_1}{4\,k_2} \sim 160 \text{ m}. \tag{3.7}$$

For comparison, the distance between the camera and the object is $b' = 120$ m.

Obviously, if $b \sim b'$ then the lighting for the scene could not have been provided by the Sun. We thus scale all distances down to 1:48, which we came to expect from the micro-motion of the Lunar Module Ascent Stage replica to find,

$$b \simeq 3.5 \text{ m, and } b' \simeq 2.5 \text{ m}. \tag{3.8}$$

3.5. Baby, you are firework!

If the entire lift-off was staged on the Earth, using 1:48 replica then the question is how it was performed.

Firstly, from the flicker caught on the video recording we conclude that the time scale was not changed.

Secondly, in order for the replica on the Earth to achieve constant acceleration, a system of cables and pulleys has to be in place with the LMAS being on one end of the cable, and some extra mass $M > m^{LM}$ on the other end. Assuming single pulley with a cable, and two masses on each side of the cable, the acceleration of the system is

$$a \simeq \frac{(M - m^{LM})\cdot g_{Earth} - F_{fr}}{M + m^{LM} + \frac{I_p}{R^2}}, \tag{3.9}$$

where I_p is the moment of inertia of the pulley and R is the radius at which the cable interacts with pulley, while F_{fr} is the friction force between the moving and the stationery parts of the contraption.

Assuming no friction and massless pulley, the target acceleration of the replica is $a_T \sim 2 \text{ m}\cdot\text{s}^{-2}/50 = 0.04 \text{ m}\cdot\text{s}^{-2}$. As $a_T/g_{Earth} \simeq 0.004 \ll 1$, we know $M = m^{LM} + \Delta m$ with $\Delta m \ll m^{LM}$ so $\Delta m/(2\,m^{LM}) \approx a_T/g_{Earth}$. We assume replica of mass $m^{LM} = 0.5$ kg so the extra mass is $\Delta m \simeq 4$ g.

The friction force will make it difficult for two masses to start moving with the target acceleration. This is because the friction force will start as static F^s_{fr} before masses start to move, then become dynamic F^d_{fr} with their motion, where $F^d_{fr} < \Delta m \cdot g_{Earth} < F^s_{fr}$. For that reason, Δm has

to be chosen so that net force that includes F^d_{fr} produces target acceleration. However, for the two masses to start moving, they have to get a push that will help them overcome static friction F^s_{fr}. In popular vernacular the hypothetical source of that push is known as the *Chinese Firecracker theory*, which fits perfectly our findings from Section 1.

Our final remark is that the hoisted replica can still be seriously perturbed by a firework exploding under its rear. As this is not shown on the video recording, we surmise that the replica could only move along a railing.

3.6. Conclusions

Analysis of the entire lift-off strongly suggests that the scene features a smaller scale replica, say 1:48, being pulled up on a stage of size ~ 4 m across. In this scaled setup, fireworks are required for the replica to overcome the static friction and to start moving with target acceleration. The stage lighting appears to be driven by 60 Hz VAC, suggesting that the studio was in the United States. That the incandescent studio ligths appear to be flickering at 5 Hz, together with the artefacts on the images similar to the edge of film stock, suggest that the entire scene is recorded with a film camera, which for some reason operated at 25 fps (European standard) and not at 24 or 30 fps (the USA standard).

3.7. Tables and Figures

Frame (s)	X (pixel)	Y (pixel)
984	204	175
985	204	175
986	204	175
987	204	175
988	204	175
989	204	175
990	205	175
991	205	177
992	205	177
993	205	176
994	205	176
995	203	175
996	204	174
997	205	174
998	205	173
999	205	174
1000	205	173
1001	205	173
1002	205	173
1003	205	173
1004	205	173
1005	205	173
1006	205	172
1007	205	172
1008	205	172
1009	205	171
1010	205	170
1011	205	170
1012	205	170

TABLE IV: X- and Y-pixel coordinates of the bottom left corner of the Lunar Module Ascent Stage in the images $[984 : 1012]_{25}$. Please note mild lateral oscillation in the frames $[994 : 997]_{25}$.

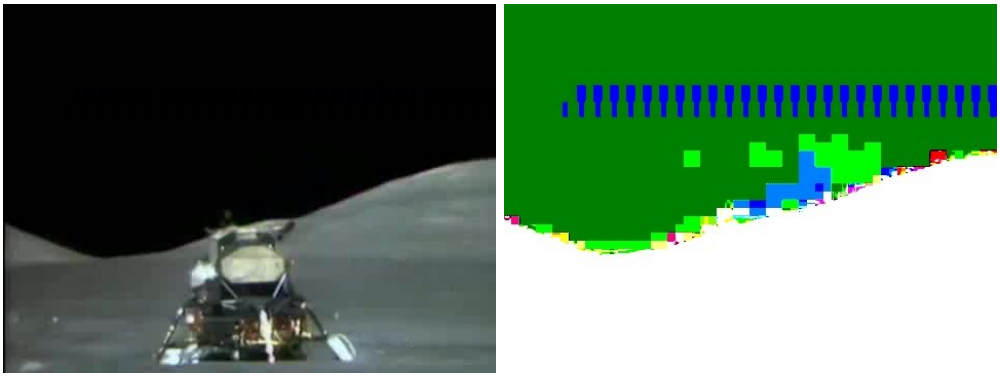

FIG. 9: The images $[681 : 685]_{25}$, with which the video-recording of liftoff actually starts (the preceeding images showing the Apollo 17 mission patch), have identical artifact that strongly resembles an edge of film stock. The left panel shows the original image 681_{25}, while the right panel shows the same image manipulated with GIMP [14], to brightness 127 and contrast 127. The artifact is clearly visible across the top half of the image.

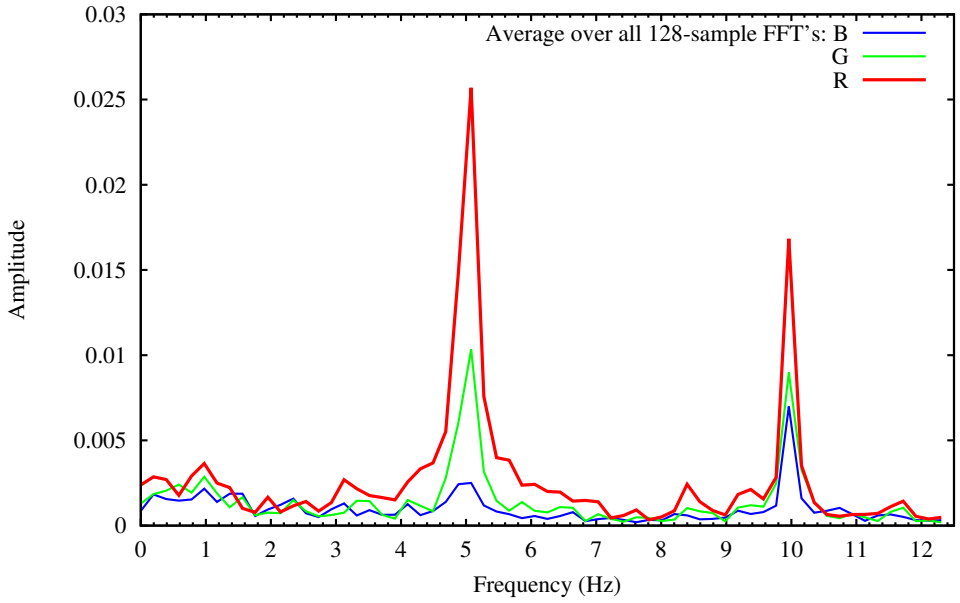

FIG. 10: Fourier Transform of the red, green and blue channels of images $[681 : 901]_{25}$ has strong 5 Hz and 10 Hz peaks. Hypothetical origins of the peaks are discussed in the text.

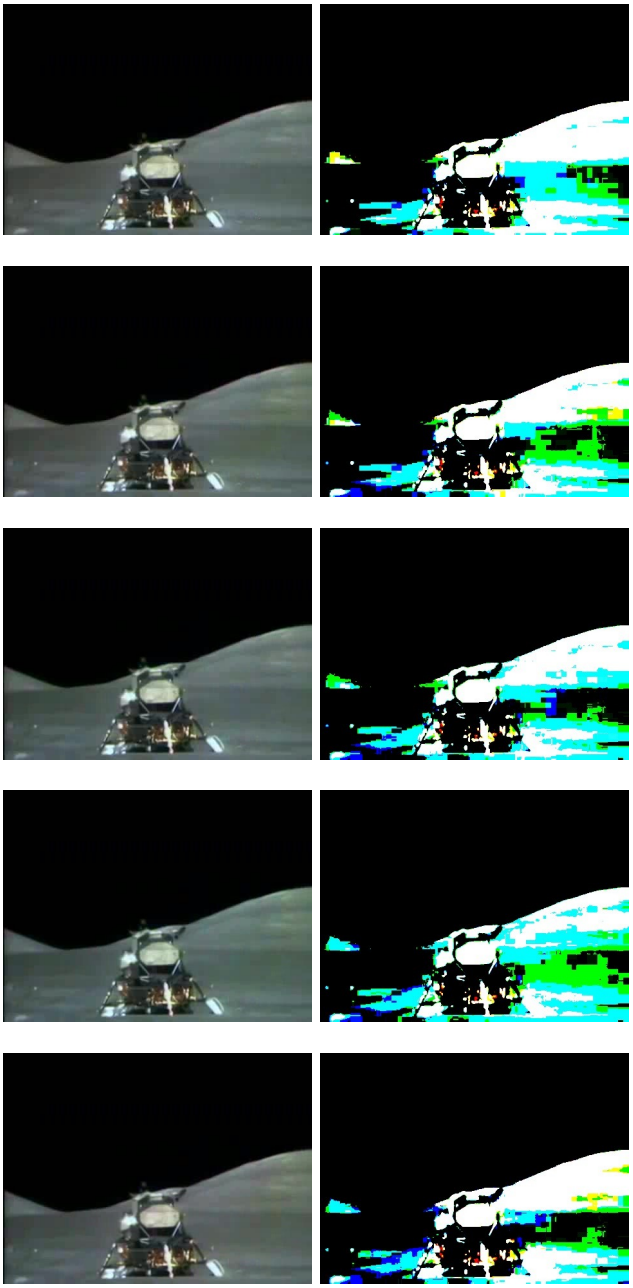

FIG. 11: 5 Hz pulsating light pattern in the images $[681:685]_{25}$ barely visible in the originals (left column) emerges after some post-processing (right column) in GIMP [14] (brightness 50 and contrast 127). The pattern comprises of peridic light fluctuations of two reflections on the ground on the right of the Lunar Module, and the brightness of the hill on the right (presumably Camelot, behind in the distance). The pattern repeats at 5 Hz (in sequences 5 images long, like the one shown) for the duration of pre-liftoff.

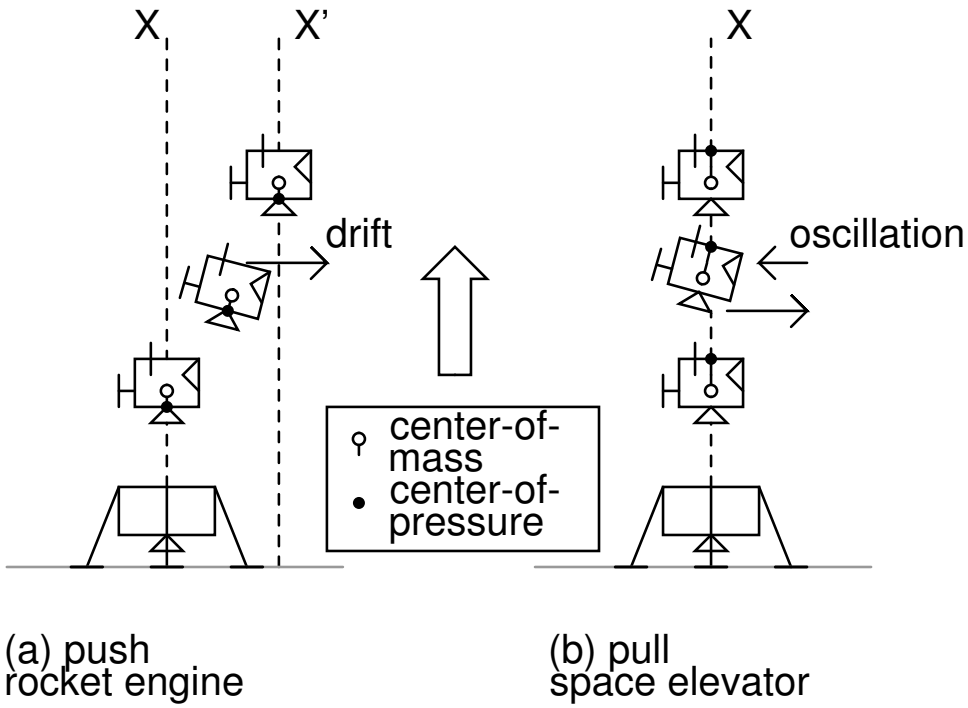

FIG. 12: Two propulsion mechanisms acting at the center-of-pressure on an object, *the push* by the rocket (left panel) and *the pull* by the rope where the center-of-pressure is constrained to vertical degree of freedom (right panel) are considered in the text. The perturbations to the motion manifest themselves differently. While under the push the object may drift sideways as the perturbations accumulate, under the pull the perturbations are self-rectifying all the while the center-of-pressure maintains its initial direction irrespective of perturbations.

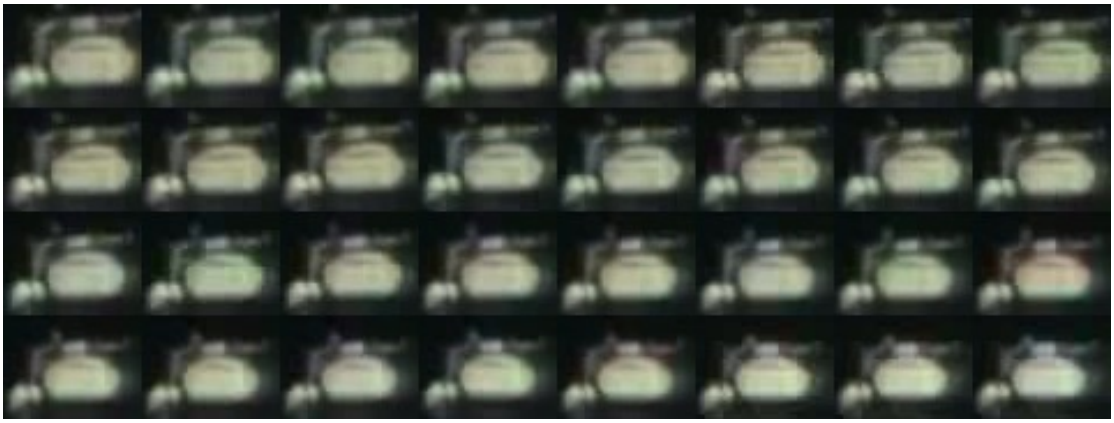

FIG. 13: 32 segments of size 61x46 pixels from the image sequence $[981 : 1012]_{25}$ of the liftoff. The segments are numbered from top to bottom, left to right, while the bottom left corner of the segment in the image is provided in Tbl. IV. Please observe that the Lunar Module Ascent Stage appears brighter as it climbs, while it size shrinks as the distance to the camera increases and because of the zoom-out, see discussion in the text.

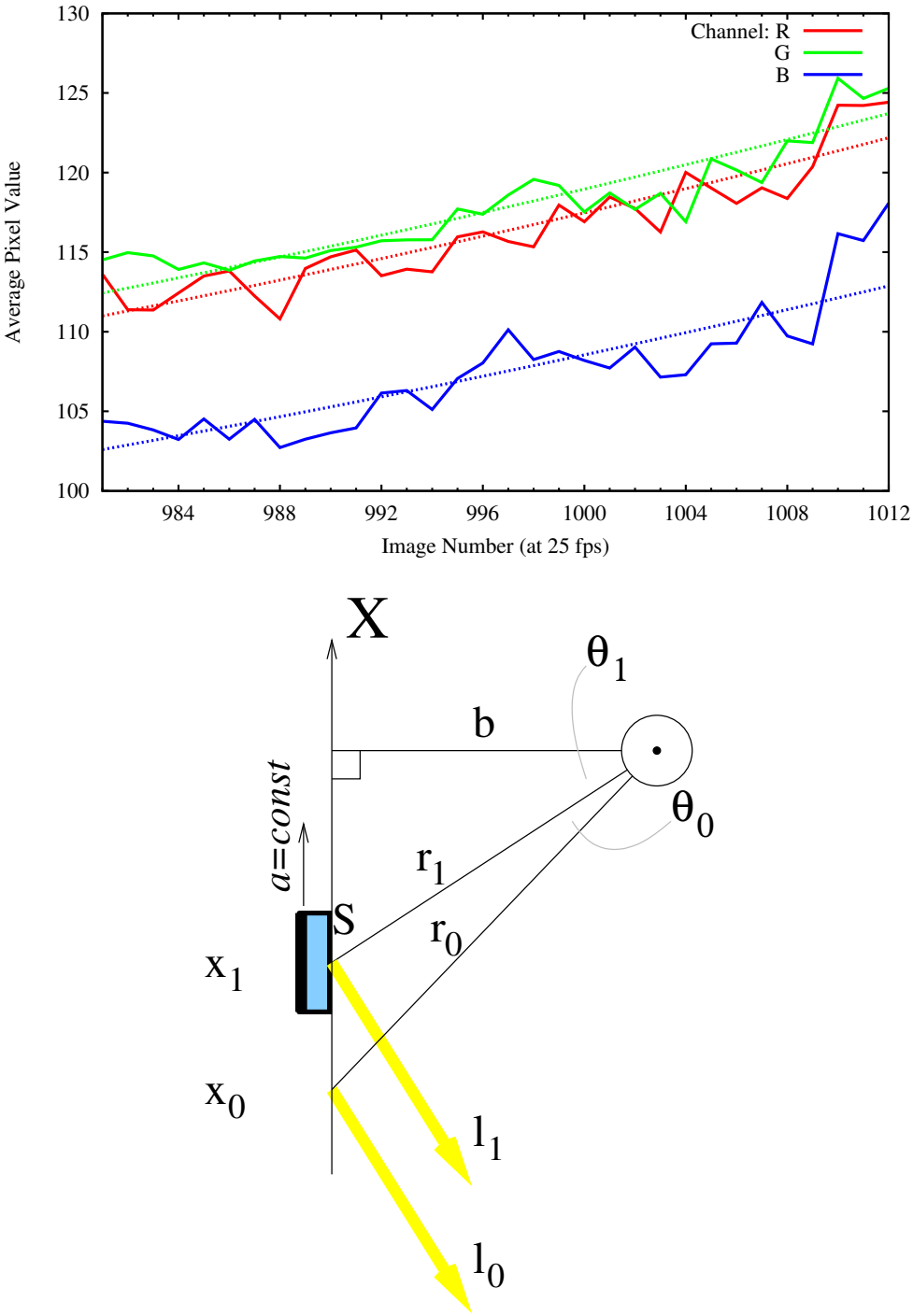

FIG. 14: (Top panel) The average pixel color channel values above cut-off $\lambda = 50$ increase as the Lunar Module Ascent Stage (LMAS) climbs. Were the LMAS illuminated by the Sun (for all practical purposes) at infinity, this should have been a constant as it represents an average illumination by the light source. (Bottom panel) The illumination of an ascending object (blue rectangle) may increase if the object is approaching the light source (astrological symbol for Sun), here at the distance b from the liftoff trajectory (coincide with the X-axis), see discussion in the text.

4. STANDING IN MOTION

In this section we discuss behavior of the lunar surface sensing probes (LSSP) in a sequence of images from Apollo 11 mission.

As is known, [7, 15] the LSSPs attached to each landing gear footpad, except the forward one, are the electromechanical devices. After deployment, the probes are extended so that the probe head is approximately 1.7 m below the footpad. When any probe touches the lunar surface, pressure on the probe head will complete (close) the circuit that advises the astronauts to shut down the descent engine.

We have seen already the landing gear in Fig. 6, which shows how the LSSP are stowed prior to landing gear deployment, while Fig. 15 shows their fully deployed position in the absence of gravity.

4.1. Cantilever Beam

For the following discussion we assume that the LSSP can be represented as an aluminum cylinder of outer radius $2 \cdot r = 2.54$ cm and inner radius $r_i \leq r$, and length $l = 1.71$ m (5'7.2"), firmly supported at the footpad end, while the other end is free. Let f be an uniform load (force per unit-length) of the beam. As is known, then the deflection of the free end of the beam δ is given by

$$\delta = \frac{f\, l^4}{8\, E\, I}, \tag{4.1}$$

where $E = 6.90 \cdot 10^{10}$ N/m^2 is the Young modulus of Aluminum, while $I = \frac{\pi}{4}(r^4 - r_i^4)$ is the area moment of the cylindrical beam cross section of outer radius r and inner radius r_i.
Consider now two cases in which the load is uniform,

1. *Yaw with uniform rate ω*
   (rotation around the LM's X-axis with constant angular velocity)
   We find load f as,

$$f^{\omega} \approx \frac{m}{l}\omega^2\, R, \tag{4.2}$$

   directed outwards. Considering that $R = 4.3$ m is the distance of the fixed end of the beam to the X-axis, we can neglect the contribution of the outward displacement δ itself to f, as

$R \gg \delta$. We find lower estimate using $r^4 - r_i^4 = (r^2 + r_i^2)\,(r^2 - r_i^2) < 2\,r^2\,(r^2 - r_i^2)$, so

$$\delta^{\omega} > \delta^{\omega}_{min} = \frac{\rho\, R\, l^4\, \omega^2}{4\, E\, r^2}, \tag{4.3}$$

where $\rho = 2,500$ kg/m^3 is the mass density of Al. We summarize the results for various ω in the following table

ω (rev/min)	δ^{ω}_{min} (cm)
0.10	0.1
0.25	0.5
0.50	2.0
0.75	4.6
1.00	8.1

2. *Yaw with uniform change of rate α for the duration of Δt*
   (Uniform angular acceleration motion)
   By the Newton 3^{rd} Axiom, tangential acceleration of the LMAS achieved by firing of its Reaction Control System (RCS) produces uniform load

$$f \simeq \frac{m}{l} \alpha\, R, \tag{4.4}$$

   on beam opposite of the direction of motion of the LMAS. After Δt the LMAS achieves angular velocity $\omega = \alpha \cdot \Delta t$. We compare two displacements as,

$$\frac{\delta^{\alpha}_{max}}{\delta^{\omega}_{min}} = \frac{f^{\alpha}}{f^{\omega}} = \frac{1}{\omega\, \Delta t} = \frac{1}{\alpha\, \Delta t^2}. \tag{4.5}$$

   It is important to recognize that the displacements δ^{α}_{max} and δ^{ω}_{min} are different in nature. Once the angular acceleration drops to zero, the displacement δ^{α}_{max} throws the deflected probes out of the equilibrium position described by the δ^{ω}_{min}, so they begin to oscillate in radial and tangential direction.

What is the Lunar Module angular acceleration α? When RCS operates at a full throttle on N nozzles, this produces total thrust of $N \cdot F = N \times 480$ N, where $N = 2$ or 4. The nozzles are located at arm length $r_{RCS} = 2.44$ m. We approximate the moment of inertia of the Lunar Module (LM) as follows. If it had uniformly distributed mass up to the distance r_{RCS}, its radial mass density

dm/dr would have been $\frac{dm}{dr}(r) = (2\,m^{LM}/r_{RCS}^2)\cdot r$, resulting in $I = \frac{1}{2}\,m^{LM}\,r_{RCS}^2$. However, we assume that the LM is loaded so that most of the mass is at the center and this linearly falls toward the edges, $\frac{dm}{dr}(r) = (2\,m^{LM}/r_{RCS}^2)\cdot(r_{RCS} - r)$, so

$$I_{LM} \simeq \frac{1}{6}\,m^{LM}\cdot r_{RCS}^2, \tag{4.6}$$

and find

$$\alpha = N\cdot\frac{r_{RCS}\,F}{I_{LM}} \simeq N\cdot\frac{6\,F}{m^{LM}\,r_{RCS}} = N\times 0.072\ \text{rad/s}^2 \simeq N\times\frac{2}{3}\ \text{rpm/s, with } N = 2,4. \tag{4.7}$$

4.2. The Hinge as Free Pivot Point

A LSSP comprises of three elements, an off-center stub welded to the footpad of length $a \simeq 0.2$ m, followed by a short beam of length $b \sim 0.3$ m, to which a beam of length $c \sim 1.5$ m is attached. The angle between beams b and c is fixed at $\gamma = 105^o$. The angle between a and b is maintained by a spring-loaded hinge that was deployed at the start of the Trans-lunar coast, and is $\sim 90^o$. For the following discussion we measure all the positions with respect to the hinge, and all angles with respect to the X-axis.

We find the deflection of the LSSP's free end assuming that the gravity in the direction of the negative X-axis is present, and that the hinge is a pivot point. Then, the LSSP will mildly flex inwards, toward the LM symmetry axis. The condition that the torque on the LSSP with respect to hinge is zero reads,

$$3\,b\,\sin\theta_{max} + c\,\sin(\pi - \gamma + \theta_{max}) = 0, \tag{4.8}$$

which solution is $\theta_{max} \simeq 131^o$. The displacement of the end of the LSSP is then $\Delta y_0 \simeq -0.45$ m, that is, inwards.

Conversely, in the absence of gravity the spring in the hinge pushes θ to $\theta_g = 105^o$, so that the LSSP is parallel with the X-axis of the LM.

We conclude that a combination of the hinge spring and the gravity puts the LSSP at an angle $\theta \in [\theta_g, \theta_{max}]$. This appears visually as the LSSP's being flexed mildly inwards toward the X-axis of the LM.

4.3. Finding Yaw Rate from Data Logs

This being said, let us consider next a series of 12 images of Apollo 11 Lunar Module AS11-44-6575 [19, 24], AS11-44-6576 [19, 25], AS11-44-6577 [19, 26], AS11-44-6578 [19, 27], AS11-44-6579 [19, 28], AS11-44-6580 [19, 29], AS11-44-6581 [19, 30], AS11-44-6582 [19, 31], AS11-44-6583 [19, 32], AS11-44-6584 [19, 33], AS11-44-6585 [19, 34], and AS11-44-6586 [19, 35], which we reproduce for reader's convenience in Fig. 16. These images capture a yaw by 360^o (1 rev) of the Lunar Module (LM) following the undocking from the Command and Service Module (CSM).

From the NASA documentation, it takes some effort to figure out over what period of time these images were taken:

- The Apollo 11 Photography Index [36], p. 93, states that the images are taken at GET 100:50 hrs. According to the The Apollo 11 Flight Plan [37] at that time the Separation between the LM and the CSM has already commenced: the Separation starts at GET 100:40 hrs and until GET 101:30 hrs does not requires any yaw changes.

- In the transcript of voice communications between the ground control and the LM and the CSM, The Apollo 11 Flight Journal [38], Armstrong mentions yaw maneuvers by the LM at GET 100:13:13 hrs, and at GET 100:19:05. During the first yaw, Collins is at the commands of the CSV trying to control the CSM roll rate and the distance from the LM - so he is not operating the camera. The second yaw maneuver goes from GET 100:19:05 hrs (Armstrong mentions word "yaw" in his communication with Collins, and goes off-line) to GET 100:20:28 hrs (Aldrin is back on line awaiting further instructions), and is of approximate duration 1 minute 20 seconds. To accomplish one revolution in that time, the yaw rate ω_2' must be

$$\omega_2' \simeq \frac{3}{4} \text{ rpm}. \tag{4.9}$$

- The Apollo 11 Flight Plan [37] lists two yaw maneuvers in the Lunar Module Flight Plan, p.3-67/190[53], which take place in the interval GET 100:15 hrs and GET 100:25 hrs, during Undocking stage. The first is 60^o ($\frac{1}{6}$ rev) left yaw, while the second is 360^o (1 rev). In the section on Lunar Module RCS Propellant Budget [37], p.5-27/319, the same two yaw maneuvers are listed as taking place at GET 100:20 hrs, with a fuel budget of $\Delta m_{p,1} = 0.77$ kg, and at GET 100:25 hrs with $\Delta m_{p,2} = 0.36$ kg. The mass burn rate of the RCS is

$\dot{m} = N \times 0.168$ kg/s, where $N = 2, 4$ is the number of nozzles used for yaw, so the durations of the burns are $\Delta t_1 = (4.58/N)$ sec, and $\Delta t_2 = (2.15/N)$ sec. Given the angular acceleration $\alpha \simeq (N \cdot \frac{2}{3})$ rpm/s, their final yaw rates are

$$\omega_{1,2} = \frac{\Delta t_{1,2}}{2} \cdot \alpha \simeq \frac{3}{2}, \ \frac{3}{4} \text{ rpm}. \tag{4.10}$$

Here, the factor $\frac{1}{2}$ means that the identical burn has to be used to zero the yaw rate.

We see that $\omega_2 \approx \omega_2'$ from Eq. (4.9), and so confirming our assumption of mass distribution in the LM. We thus conclude that The Apollo 11 Flight Plan entries for the 360^o yaw are consistent with the voice communications between the crew and the ground control providing that the yaw rate was

$$\omega \simeq \frac{3}{4} \text{ rpm}. \tag{4.11}$$

For this yaw rate, the lower bound on the minimal displacement of the Lunar Surface Sensing Probe (LSSP) free end is

$$\delta^{\omega}_{min} \gtrsim 5 \text{ cm}, \text{ radially outwards}, \tag{4.12}$$

On the other hand, we find $\delta^{\alpha}_{max} \gtrsim 58$ cm, which is too great given the duration of the maneuver, $\frac{1}{2}\Delta t_2 = 1.07$ s. This simply means that the free end of the LSSP remains stationary while the footpad is accelerating away from it. We find the angular displacement of the footpad for the duration of acceleration as $\theta = \frac{1}{2}\,\alpha(\Delta t_2/2)^2 = N \times 0.04$ rad, with $N = 2$ or 4, so the LSSP free end for the duration of acceleration tangentially trails the footpad by

$$\delta^{\alpha} \simeq \theta \cdot R \geq 18 \text{ cm}. \tag{4.13}$$

Upon completion of the burn, the LSSP's continue to oscillate around their equilibrium positions, and these oscillations should be particularly visible after the start and after the end of the 360^o yaw.

4.4. Results and Discussion

As can be seen from all the images in Fig. 16, and in particular in Fig. 17, the Lunar Surface Sensing Probes are always flexed mildly inwards, without any radial or tangential motion, or hint thereof.

The LSSP's being flexed inwards suggests in identical fashion in all the images is consistent with the LM being stationary and suspended in the presence of gravity, in stark contrast to what it was supposed to be doing (yawing) and where (in a circular orbit around the Moon where it would appear weightless).

One could hypothesize that the images could have been taken while the LM was stationary and the CSM was moving around it in a circle facing the LM. However, that would have been quite a complicated maneuver for Collins to perform with the CSM considering the computational resources and the available time he had at his disposal, while simultaneously standing by the window and operating the camera.

From the patterns of the Kapton tape (thickness, spacing and position) on the primary struts shrink wrapping, it is clear that the same LM is featured here and on the Moon. We thus conclude that what is depicted in Fig. 16 is consistent with the entire scene being part of a greater act in which the life-size replica of the LM is lowered down to the stage representing the Moon. While the LM is suspended in the air, the stage lights are pointed at the LM's bottom. A camera operator walks around on a platform surrounding the stage and occasionally takes pictures - initially more frequently, while later at steady rate of 1 picture per 1/4 turn. This then also explains why the primary struts are un-deployed: later on the LM is gently lowered down to the stage.

We believe that the disconnect between the real achievements of the Apollo 11 mission and - what we suggest are - its staged parts, is well documented in two series of images:

1^{st} Series comprise the images AS11-36-5310 [19, 39], AS11-36-5311 [19, 40], AS11-36-5312 [19, 41], AS11-36-5313 [19, 42], AS11-36-5314 [19, 43], AS11-36-5315 [19, 44] and AS11-36-5316 [19, 45], which were taken at GET 3:15 hrs through GET 3:25 hrs at the beginning of the Trans-Lunar Coast (TLC) as the rocket is moving radially away from the Earth and passing through Van Allen Belts. After the CSM separates from the Saturn IV-B rocket, it turns around and docks with the LM still attached to the rocket. The images in this series feature the detailed views of the top of the LM as seen from the approaching CSM, where the LM appears to be illuminated sideways by the Sun. The camera is set to low light conditions, so the pictures capture the brightest stars, as well, cf. AS11-36-5310. The images

featuring the Saturn IV-B rocket with Earth in the background are conspicuously absent, even though Earth center is some 26,000 km away (and Earth is of diameter of some 13,000 km) and Earth should be more then half bright from the TLC trajectory.

2^{nd} Series comprise the images AS11-44-6565 [19, 46], AS11-44-6566 [19, 47], AS11-44-6567 [19, 48] and AS11-44-6568 [19, 49], which were taken at the start of Undocking around GET 100 hrs. The Apollo 11 has just passed behind the Moon on its last orbit before undocking, and two separate spacecrafts re-emerged. They would make one further lunar orbit, then the Lunar Module would enter its descent orbit. The images should show the top of the LM in similar lighting conditons as in the 1^{st} Series, but now the specular reflection of the light from the CSM is present, as well. The camera is set to bright light conditions, so no stars are captured.

The indentations and the markings on the top surface of the LM in two series of images, strongly suggest that these are two distinct LM.

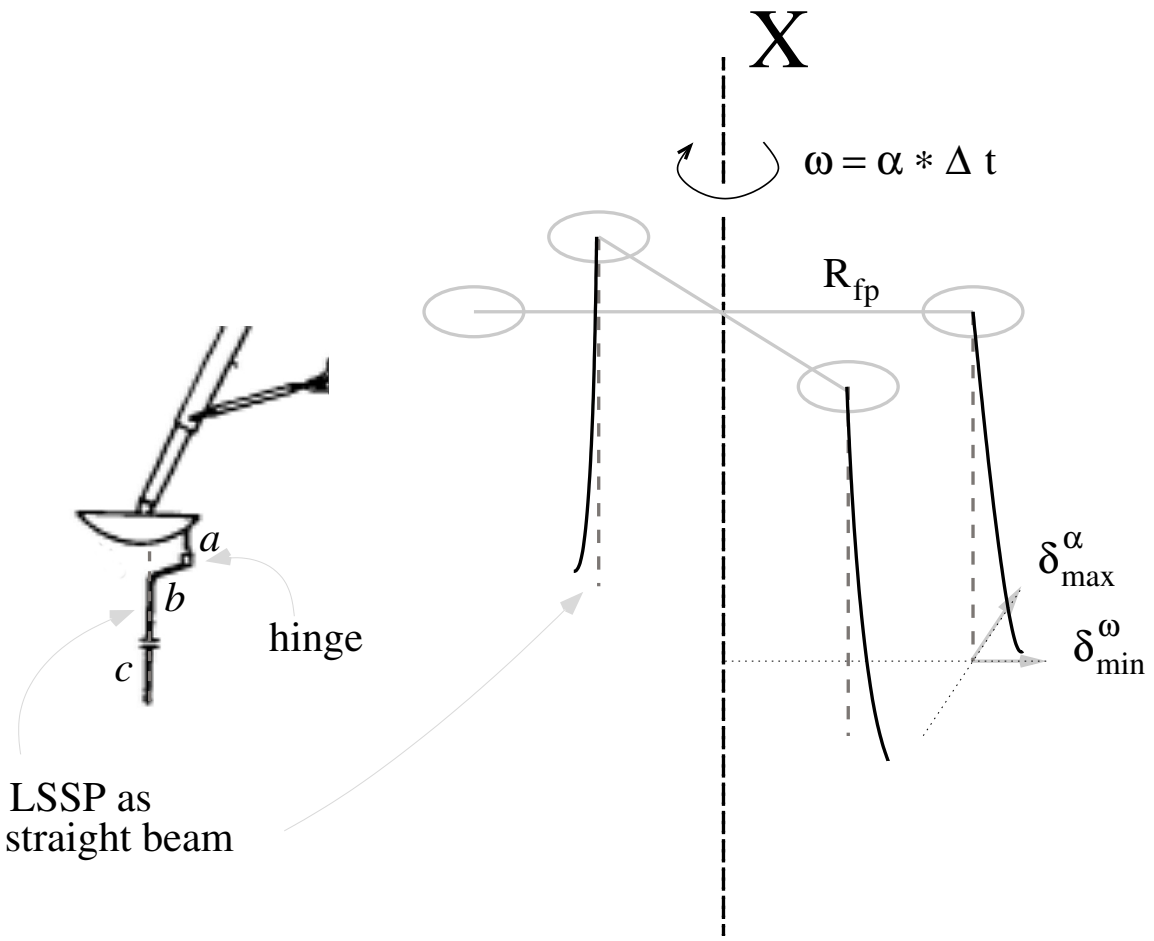

FIG. 15: (Left insert) Fully deployed Lunar Surface Sensing Probe (LSSP), [15] is attached to the footpad through a spring-loaded hinge, which fixes the probe in the landing position, in which the segment c is parallel with the X-axis of the Lunar Module.
(Right panel) In yawing Lunar Module assuming the rigid landing gear, the Lunar Surface Sensing probes are deflected tangentially (lagging behind by δ^{α}_{max} for duration of the acceleration) and radially (outwards by at least δ^{ω}_{min} because of centrifuge effect). The Lunar Module uses the Reactive Propulsion System (RPS) to reach ω through α for the duration Δt.

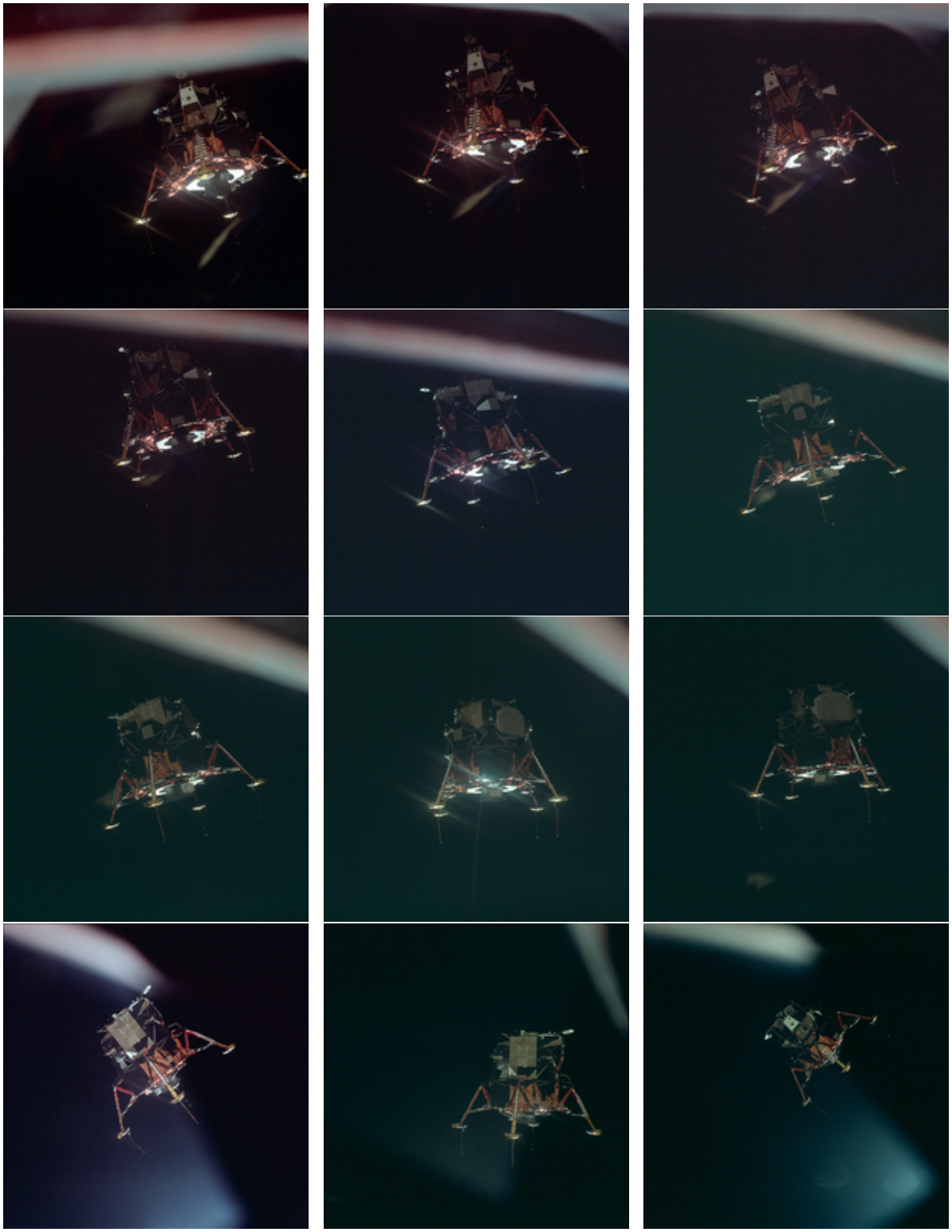

FIG. 16: In the 12 image sequence, AS11-44-6575 to AS11-44-6586 (left to right, top to bottom, all rotated by 90^o clockwise with respect to the hyper-linked original images at the Lunar Planetary Institute), the Apollo 11 Lunar Module (LM) yaws clockwise (left screw) by one revolution in front of the Control and Service Module. The 360^o yaw was part of the LM Inspection during the Undocking and Separation Stage, and it took place around GET 100 hr when both vessels were presumably in a circular orbit around the Moon. Notice that the Lunar Surface Sensing Probes maintain fixed position with respect to the LM X-axis and the landing gear.

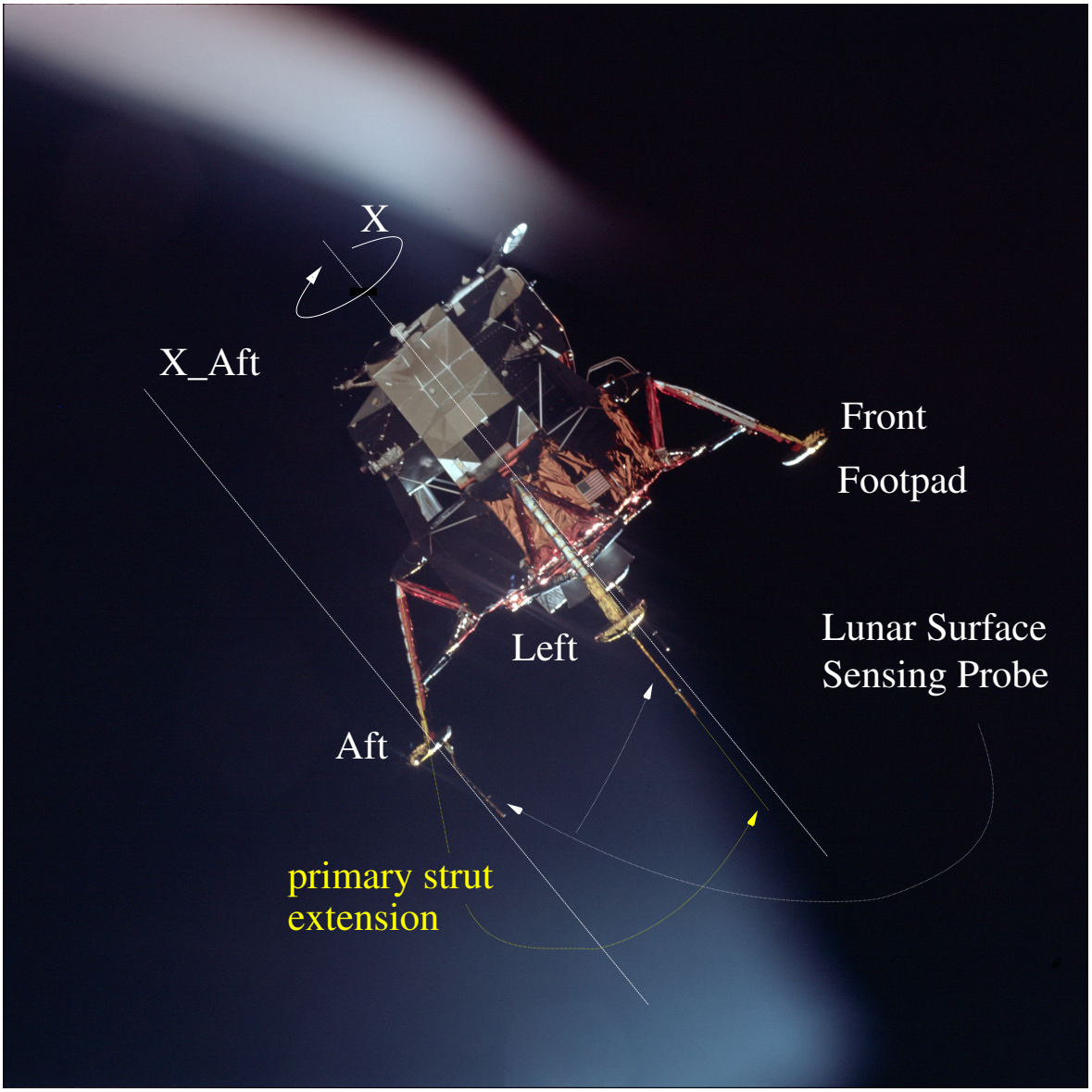

FIG. 17: The image AS11-44-6584 (rotated by 90^o clockwise with respect to the original at the Lunar Planetary Institute) from the seqence in Fig. 16 shows the yawing Lunar Module. The Aft Lunar Surface Sensing Probe (LSSP) is flexed mildly inward with respect to the LM X-axis (and its parallel through Aft footpad X_Aft), while the movement (or indication of it) of all probes in radial and tangential direction is conspicuously absent. The Left LSSP coincides with the line extending through the primary strut, and thus shows no lateral displacement that could be attributed to an earlier tangental acceleration of the LM. For comparison, in Fig. 15 we show how the yaw rate affects the LSSP's displacements.

5. I KNOW YOU CAN'T FAKE IT ANYMORE

We have investigated four scenes from the body of evidence that NASA presented in support of their claim that they flew to the Moon, namely (i), the dynamics of Apollo 17 lift-off; (ii), the deployment of primary struts during the Moon landing of the Apollo 11 and Apollo 17 missions; (iii), the illuminance of the Ascent Stage in the video recording of Apollo 17 of lift-off; and (iv), the flexing of the Lunar Surface Sensing Probes during a yaw maneuver in circular Moon orbit prior to descent orbit insertion. We have chosen the scenes based on the physical mechanisms at play were they recorded on the way to the Moon. In all instances we find serious discrepancies between the stresses on the Lunar Module depicted in the scenes and NASA's own performance specifications. In fact, the discrepancies are so great that the findings reported in the previous four sections fully support the alternative explanation that emerged in the public in the last two decades, namely, that the pictures of the Lunar Landings and the Lift-offs were staged and recorded on Earth.

Acknowledgments

The author acknowledges discussions with anonymous NASA employees to determine when the Lunar Module 360^o yaw took place and how much fuel it consumed: In those discussions it was hypothesized that the entries in the Lunar Module Flight Plan for the two yaw burns might have been interchanged by mistake (first of 60^o, second of 360^o, where the first uses more fuel then the second, see Sec. 4 for full analysis assuming that the log entries are in correct order).

The author acknowledges that the section and subsection titles are titles of or verses from the musical pieces, "Fly Me to the Moon," by Bart Howard (performed by Frank Sinatra), "Let's Twist Again," by Kal Mann and Dave Apell (performed by Chubby Checkers), "Shake a Leg," by AC/DC, "Also Sprach Zarathustra," by Richard Strauss, "Firework," by Katy Perry, "Standing in Motion," by Yanni, and "A New Door," by Lenny Kravitz.

[1] NASA, *Apollo 17 Traverse Planning Data, 3rd Edition*, Fig. 23 on p. 97, [Online; accessed January 18, 2014], URL https://www.hq.nasa.gov/alsj/a17/A17TraversePlanningData.pdf.

[2] NASA, *Apollo 17 Traverse Planning Data, 3rd Edition*, Fig. 7A on p. 15, [Online; accessed January 18, 2014], URL https://www.hq.nasa.gov/alsj/a17/A17TraversePlanningData.pdf.

[3] Smithsonian National Air and Space Museum, *Camera, Television, Lunar Rover, Apollo*, Retrieved May 16, 2014 from http://airandspace.si.edu/collections/artifact.cfm?object=nasm_A19850021000.

[4] S. T. Thornton and J. B. Marion, *Classical Dynamics of Particles and Systems* (Brooks/Cole, Belmont CA, 2004), chap. 9, 5th ed.

[5] S. Glasstone, *Sourcebook on the Space Sciences* (D. Van Nostrand Company, Inc., 1965), (Ch. 3).

[6] J. C. M. IV and J. K. Allred, in *45th AIAA/ASME/ASEE Joint Propulsion Conference and Exhibit* (Denver, Colorado, USA, August 2-5, 2009).

[7] Apollo News Reference, *Lunar Module Quick Reference Data*, Retrieved June 25, 2015 from https://www.hq.nasa.gov/alsj/LM04_Lunar_Module_ppLV1-17.pdf .

[8] Wikipedia, *Apollo Lunar Module*, Retrieved April 12, 2015 from https://en.wikipedia.org/wiki/Apollo_Lunar_Module .

[9] Robert A. Braeunig, *Lunar Module Ascent Simulation* (2009), Retrieved April 11, 2010 from http://www.braeunig.us/apollo/LM-ascent.htm, URL http://www.braeunig.us/apollo/LM-ascent.pdf.

[10] Youtube Apollo Houston Channel, *Apollo 17 Lunar Liftoff HD (Inside and Outside view)*, Retrieved June 25, 2015 from https://www.youtube.com/watch?v=XlGis35Epvs .

[11] *Clip Converter - Free Online Media Conversion and Download*, http://www.clipconverter.cc.

[12] The FFmpeg developers, *FFmpeg 2.6.1* (2015), https://www.ffmpeg.org.

[13] Jennifer Levasseur, *Leaving the Moon, Watching at Home* (2011), [Online; accessed January 18, 2014], URL http://http://blog.nasm.si.edu/history/leaving-the-moon-watching-at-home/.

[14] The GIMP Team, *GNU Image Manipulation Program* (2015), https://www.gimp.org.

[15] NASA, *Apollo Operations Handbook - Lunar Module LM 10 and Subsequent - Volume I - Subsystems Data* (1970), [Online; accessed January 18, 2014], URL https://www.hq.nasa.gov/alsj/alsj-LMdocs.html.

[16] ApolloHoax.net, *Topic: Apollo 17 ascent module liftoff* (2014), [Online; accessed January 11, 2015], URL http://www.apollohoax.net/forum/index.php?topic=655.0.

[17] TRW Systems Group, *LMAGS Operating Manual - Flight Program 6* (1969), [Online; accessed January 18, 2014], URL https://www.hq.nasa.gov/alsj/alsj-LMdocs.html.

[18] Robert F. Stengel, J. Spacecraft and Rockets **7**, 941 (1970), Presented as Paper 69-892 at the AIAA Guidance, Control and Flight Mechanics Conference, Princeton, NJ, August 18-20, 1970.

[19] Lunar Planetary Institute, *Apollo Image Atlas: 70mm Hasselblad*, [Online; accessed July 13, 2009], URL http://www.lpi.usra.edu/resources/apollo.

[20] Lunar Planetary Institute, *AS11-40-5921*, SHA1SUM: b899ebaa972c2680ad2e0a6e5fd90e3152ac92bb, URL http://www.lpi.usra.edu/resources/apollo/images/print/AS11/40/5921.jpg.

[21] Lunar Planetary Institute, *AS11-40-5927*, SHA1SUM: 75f51ac6d2fe6f2291f7b72d73a983f7c897d4d5, URL http://www.lpi.usra.edu/resources/apollo/images/print/AS11/40/5927.jpg.

[22] P. T. Metzger, C. D. Immer, C. M. Donahue, B. M. Vu, R. C. Latta, III, and M. Deyo-Svendsen, ArXiv e-prints (2009), Journal reference J. Aerospace Engineering Vol. 21, No. 1, January 2009, pp. 24-32, 0906.0196, URL http://arxiv.org/pdf/0906.0196v1.

[23] F. Pitié, Master's thesis, Trinity College, Dublin, Ireland (2002), [Online; accessed January 11, 2015], URL http://citeseerx.ist.psu.edu/viewdoc/download?doi=10.1.1.1.1574.pdf.

[24] Lunar Planetary Institute, *AS11-44-6575*, SHA1SUM: 7698ccfab214c3aca045ae1d8ce40ef7be8bb9bf, URL http://www.lpi.usra.edu/resources/apollo/images/print/AS11/44/6575.jpg.

[25] Lunar Planetary Institute, *AS11-44-6576*, SHA1SUM: 776f462ac9f082d71a98d5ed5570c4184fcedbe3, URL http://www.lpi.usra.edu/resources/apollo/images/print/AS11/44/6576.jpg.

[26] Lunar Planetary Institute, *AS11-44-6577*, SHA1SUM: 79e913ca016c445b673d0d7df7dcd595e5e45f5b, URL http://www.lpi.usra.edu/resources/apollo/images/print/AS11/44/6577.jpg.

[27] Lunar Planetary Institute, *AS11-44-6578*, SHA1SUM: 14a2d98a627cd6e6bf07a25a5d6700509c948dc6, URL http://www.lpi.usra.edu/resources/apollo/images/print/AS11/44/6578.jpg.

[28] Lunar Planetary Institute, *AS11-44-6579*, SHA1SUM: 183798d022bf1349ff58822c562dd3bb9e9b1dc6, URL http://www.lpi.usra.edu/resources/apollo/images/print/AS11/44/6579.jpg.

[29] Lunar Planetary Institute, *AS11-44-6580*, SHA1SUM: ba78d904864570e10d0534b5ecdc043cd0868ce4, URL http://www.lpi.usra.edu/resources/apollo/images/print/AS11/44/6580.jpg.

[30] Lunar Planetary Institute, *AS11-44-6581*, SHA1SUM: 7519de3468bf605b6ba8487e8ce5bd199ae81196, URL http://www.lpi.usra.edu/resources/apollo/images/print/AS11/44/6581.jpg.

[31] Lunar Planetary Institute, *AS11-44-6582*, SHA1SUM: 95a988a07b8997570eedd8a2ed366b16d39a3636, URL http://www.lpi.usra.edu/resources/apollo/images/print/AS11/44/6582.jpg.

[32] Lunar Planetary Institute, *AS11-44-6583*, SHA1SUM: bc34471a18838d4a7ef3274e3172bf802429ca70, URL http://www.lpi.usra.edu/resources/apollo/images/print/AS11/44/6583.jpg.

[33] Lunar Planetary Institute, *AS11-44-6584*, SHA1SUM: 0c4c7fb13a80a7606f7c9faed26ffada32cbb8d6, URL http://www.lpi.usra.edu/resources/apollo/images/print/AS11/44/6584.jpg.

[34] Lunar Planetary Institute, *AS11-44-6585*, SHA1SUM: 26f4c032d391bc692e8499e114293039ac13be83, URL http://www.lpi.usra.edu/resources/apollo/images/print/AS11/44/6585.jpg.

[35] Lunar Planetary Institute, *AS11-44-6586*, SHA1SUM: 51e276ad58b1ad1c738f0d89eae690ca9e0ec713, URL http://www.lpi.usra.edu/resources/apollo/images/print/AS11/44/6586.jpg.

[36] NASA, *Apollo 11 Photography Index 70 mm and 16 mm* (1969), [Online; accessed January 18, 2014], URL http://apollo.sese.asu.edu/SUPPORT_DATA/ap11_index_new.pdf.

[37] NASA, *Apollo 11 Flight Plan* (1969), [Online; accessed January 18, 2014], URL `https://www.hq.nasa.gov/alsj/alsj-LMdocs.html`.

[38] NASA, *Apollo Flight Journal: Day 5, part 2: Undocking and the Descent Orbit* (Last updated 2013-08-11), [Online; accessed January 18, 2014], URL `http://http://history.nasa.gov/ap11fj/15day5-undock-doi.htm`.

[39] Lunar Planetary Institute, *AS11-36-5310*, SHA1SUM: 7f0dea214171c7003408ebb67e411d16f8b0ba1d, URL `http://www.lpi.usra.edu/resources/apollo/images/print/AS11/36/5310.jpg`.

[40] Lunar Planetary Institute, *AS11-36-5311*, SHA1SUM: 816fcaf2dcba86c7ed9186c3ee875102799f2863, URL `http://www.lpi.usra.edu/resources/apollo/images/print/AS11/36/5311.jpg`.

[41] Lunar Planetary Institute, *AS11-36-5312*, SHA1SUM: 10f7edffaeb830e5b94bd2a74f0a6eaf10479c92, URL `http://www.lpi.usra.edu/resources/apollo/images/print/AS11/36/5312.jpg`.

[42] Lunar Planetary Institute, *AS11-36-5313*, SHA1SUM: 26cd6ce4c02a07b68ce4e18d24669ad1c7004883, URL `http://www.lpi.usra.edu/resources/apollo/images/print/AS11/36/5313.jpg`.

[43] Lunar Planetary Institute, *AS11-36-5314*, SHA1SUM: 170ce4674b988823f8cb9d5f0632796569c37146, URL `http://www.lpi.usra.edu/resources/apollo/images/print/AS11/36/5314.jpg`.

[44] Lunar Planetary Institute, *AS11-36-5315*, SHA1SUM: 1fe905186040196f8e706380d8c66c37f8385eed, URL `http://www.lpi.usra.edu/resources/apollo/images/print/AS11/36/5315.jpg`.

[45] Lunar Planetary Institute, *AS11-36-5316*, SHA1SUM: 477a41e2315e42892ada83ceaa100f82bebfb44b, URL `http://www.lpi.usra.edu/resources/apollo/images/print/AS11/36/5316.jpg`.

[46] Lunar Planetary Institute, *AS11-44-6565*, SHA1SUM: d6e94f733800a4f41456b13fa9dc6b1b40fea565, URL `http://www.lpi.usra.edu/resources/apollo/images/print/AS11/44/6565.jpg`.

[47] Lunar Planetary Institute, *AS11-44-6566*, SHA1SUM: db24785c53729a4c47e144dea6f3779528d186b2, URL `http://www.lpi.usra.edu/resources/apollo/images/print/AS11/44/6566.jpg`.

[48] Lunar Planetary Institute, *AS11-44-6567*, SHA1SUM: 2c6a350b1f89004e8fa186c972f7a6395e564886, URL `http://www.lpi.usra.edu/resources/apollo/images/print/AS11/44/6567.jpg`.

[49] Lunar Planetary Institute, *AS11-44-6568*, SHA1SUM: c23e9d65a737e722692ad2beb8f67404a1ccc5bf, URL `http://www.lpi.usra.edu/resources/apollo/images/print/AS11/44/6568.jpg`.

[50] Created using command line interface as follows,
`ffmpeg -i Apollo_17_Lunar_Liftoff_high.avi -q:v 1 -r 10 image-%05d.jpg`

[51] We use `matlab` notation throughout the report where ":" is used to designate integer range first number to second number, inclusive of the boundaries. E.g., in that notation [100 : 102] represents an array $[100, 101, 102]$.

[52] Created using command line interface as follows,
`ffmpeg -i Apollo_17_Lunar_Liftoff_high.avi -q:v 1 -r 25 image-%05d.jpg`

[53] The format p.3-67/190 refers to p.3-67 with respect to the native document pagination. As the document is provided as a PDF file, the same page is the 190^{th} from the beginning of the document.